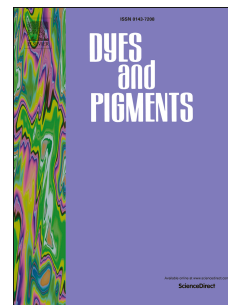


Accepted Manuscript

Facile synthesis of β -functionalized “push-pull” Zn(II) porphyrins for DSSC applications

Kamal Prakash, Shweta Manchanda, Vediappan Sudhakar, Nidhi Sharma, Muniappan Sankar, Kothandam Krishnamoorthy



PII: S0143-7208(17)31109-9

DOI: [10.1016/j.dyepig.2017.07.053](https://doi.org/10.1016/j.dyepig.2017.07.053)

Reference: DYPI 6142

To appear in: *Dyes and Pigments*

Received Date: 12 May 2017

Revised Date: 19 July 2017

Accepted Date: 21 July 2017

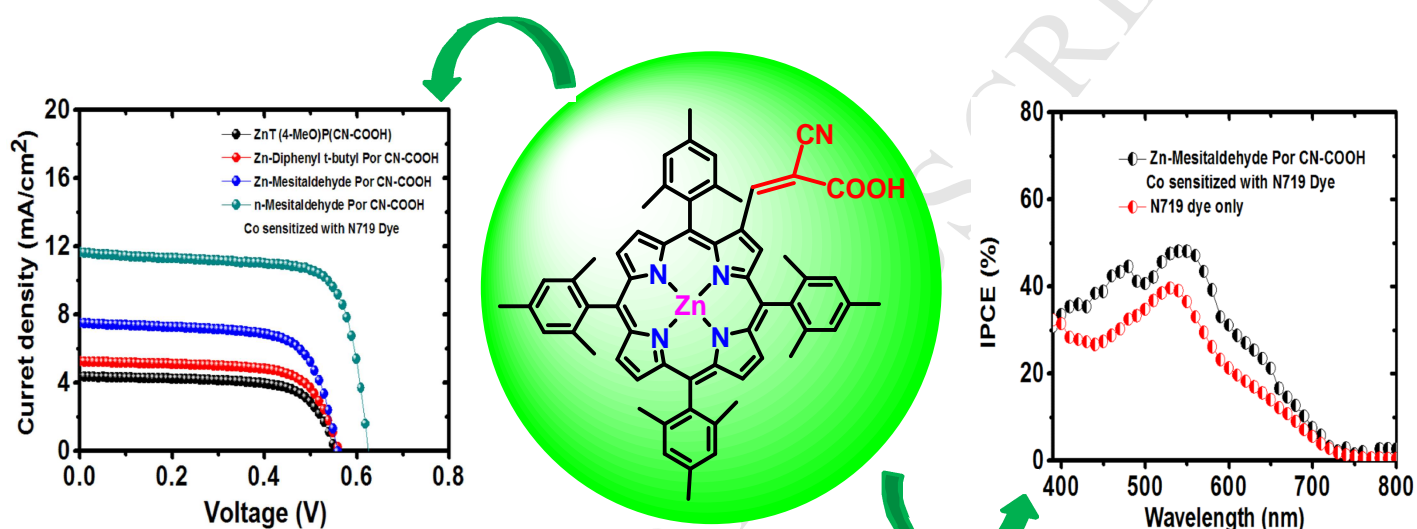
Please cite this article as: Prakash K, Manchanda S, Sudhakar V, Sharma N, Sankar M, Krishnamoorthy K, Facile synthesis of β -functionalized “push-pull” Zn(II) porphyrins for DSSC applications, *Dyes and Pigments* (2017), doi: 10.1016/j.dyepig.2017.07.053.

This is a PDF file of an unedited manuscript that has been accepted for publication. As a service to our customers we are providing this early version of the manuscript. The manuscript will undergo copyediting, typesetting, and review of the resulting proof before it is published in its final form. Please note that during the production process errors may be discovered which could affect the content, and all legal disclaimers that apply to the journal pertain.

Facile synthesis of β -Substituted “Push-Pull” Zn(II) Porphyrins for DSSC Applications

Kamal Prakash, Shweta Manchanda, VEDIAPPAN SUDHAKAR, Nidhi Sharma, Muniappan Sankar and Kothandam Krishnamoorthy

β -Functionalized “push-pull porphyrin” dyes have been designed, synthesized and studied for DSSC applications. These dyes displayed power conversion efficiency (PCE) of $\eta = 1.72$ -3.13% where co-sensitized ZnT(Mes)P(CN-COOH)(N719) dye demonstrated maximum PCE efficiency up to 5.35%, with a J_{sc} of 11.8 mA cm⁻², a V_{oc} of 630 mV and a fill factor (FF) of 0.72.



Facile Synthesis of β -Functionalized “Push-Pull” Zn(II) Porphyrins for DSSC Applications

Kamal Prakash,^a Shweta Manchanda,^a VEDIAPPAN SUDHAKAR,^b Nidhi Sharma,^a Muniappan Sankar*^a and Kothandam Krishnamoorthy*^b

ABSTRACT

Three new β -substituted “push-pull” Zn(II) porphyrin dyes with various electron donors at *meso*-positions and cyanoacetic acid as acceptor at β -position have been designed and synthesized. These porphyrins have been characterized by UV-Vis, Fluorescence, ¹H NMR and ¹³C NMR spectroscopic techniques and cyclic voltammetric studies. The Soret and Q band of Zn(II) porphyrin dyes were found to be red-shifted (30-35 nm) as compared to ZnTPP. The fluorescence quenching and the decrement in quantum yield and lifetime suggest intramolecular charge transfer from donor to acceptor. Zn porphyrin exhibited anodic shift in their first redox potentials (0.03-0.11 V) as compared to ZnTPP. The HOMO-LUMO energy levels of Zn porphyrin dyes were compared with the conduction band of TiO₂ and the electrolyte I⁻/I₃⁻. The HOMO levels of all the dyes are sufficiently higher than the energy level of electrolyte I⁻/I₃⁻ and LUMO levels significantly lower than the conduction band of TiO₂ which reflect the feasibility of facile electron-transfer. ZnT(Mes)P(CN-COOH) has been co-sensitized with N719 dye to further improve the PCE efficiency. These dyes displayed power conversion efficiency (PCE) of $\eta = 1.72$ -3.13% where co-sensitized ZnT(Mes)P(CN-COOH) (N719) dye demonstrated maximum PCE efficiency up to 5.35%, with a J_{sc} of 11.8 mA cm⁻², a V_{oc} of 630 mV and a fill factor (FF) of 72% due to better light harvesting capacity.

1. Introduction

As the global energy demand increased from the last decades, there is an urgent requirement to look for new sustainable and renewable energy sources to fulfil the advance energy demand for the next generation.¹⁻³ Silicon based solar cells have been developed for the alternate energy source but its production cost is very high. Dye sensitized solar cells (DSSC) were aroused as favourable candidate for green and clean energy due to their high efficiency and low cost of production and turn out better alternate to the Si based solar cells.¹⁻³ Traditionally, Ruthenium-based sensitizers have been utilized for DSSC to achieve high power conversion efficiency up to 11% but these complexes are expensive, rare, need skillful synthesis as well as hazardous to the environment which restrict their commercial application.^{4,5} From this point of view, tremendous efforts have been made to design and synthesize new, cost-effective, high yield and efficient metal free sensitizers.⁶⁻⁹ Many organic dyes such as perylene,¹⁰ BODIPY,¹¹ diimide,¹² coumarins,¹³ triarylamines¹⁴ and carbazole¹⁵ also reported as efficient sensitizers for DSSC with power conversion efficiency in the range 5-9% due to their comparable cost, high yield synthesis, stability and large molar absorption coefficients. Among the various type of sensitizers, porphyrin and phthalocyanine derivatives are gained much more importance as potential sensitizers for DSSC applications.¹⁶⁻²⁰ Porphyrinoids play crucial role to sustain life in living organism such as chlorophyll in green leaves, heme protein in red blood cells etc.^{21,22} Chlorophyll in green leaves absorb light from the sun for the process of photosynthesis to convert photon energy into chemical energy. In this regard, porphyrins and phthalocyanine have attracted much interest for researchers as they can be mimicked of neutral photosynthetic architectures.^{23,24} Porphyrins have intense absorptions in the visible region due to their π -conjugated aromatic system. They are easy to synthesize and functionalize at *meso*- and β -pyrrole positions which lead to interesting electronic spectral and electrochemical redox properties.²⁵⁻²⁸ Porphyrins can be synthesized in very high yield, have facile synthetic routes as well as cheaper and environmental friendly as compared to Ru-based dyes.

Porphyrins, first reported as sensitizers for DSSC by Grätzel and co-workers in 1991.²⁹ Since then, porphyrins have emerged as a class of promising molecules as DSSC materials and a lot of research has been carried out on them to achieve high power conversion efficiency for solar cells.³⁰⁻³³ D- π -A type structures have electron-donor (D), π -linker (π), and an electron-acceptor anchor (A) which enhance their photophysical properties and efficient electron injection due to intramolecular charge transfer (CT). From last few years, many *meso*-substituted push-pull porphyrins were reported with high PCE where different donor group and acceptor carboxylic acceptor group situated at opposite *meso*-positions.³⁴⁻³⁷ The zinc porphyrin sensitizer **YD2-o-C8** and **SM315** exhibited an impressive PCE of 12-13% using a cobalt-based electrolyte.^{38,39} The extension of porphyrin macrocycle can be achieved by functionalization of porphyrin at *meso*-position with promising chromophores such as acene or pyrene by increasing number of aromatic groups in the porphyrin core is a good strategy to extend the absorption spectra to greater wavelength. Fluorene-substituted sensitizer **LD22**⁴⁰ showed high PCE value of 8.1% and pyrene-substituted sensitizer **LD4**⁴¹ exhibited PCE of 10.1%, suggesting that they showed good light-harnessing capability in the near IR and visible regions. Imahori and co-workers studied the *meso*-naphthyl fused porphyrin dyes

namely **fused-ZnP1** with η -value of 4.1% which is found to be much greater than non-fused porphyrin dye **ZnP1**.⁴² Porphyrin array has been developed for DSSC solar cell due to their excellent light harvesting ability. Diao and co-workers synthesized **YDD0** and **YDD1** porphyrin dimer with η -value of 4.07% and 5.23%, respectively.⁴³ However, porphyrin arrays enhance their light harvesting ability as compared to monomeric porphyrins whereas the possibility of reduced electron ejection and dye aggregation lowers the η -value of these arrays. Co-sensitization is a key tool to enhance the DSSC performance by combining two or more dyes with complementary spectral features sensitized on semiconductor surface together which extend the light harvesting ability as well as increase photocurrent of device. Firstly, Grätzel and co-workers reported porphyrin/organic dye co-sensitization in 2010 where **YD-2** co-sensitized with an organic dye which showed an enhanced device performance of $\eta=6.9\%$ as compared to individual porphyrin dye, $\eta = 5.6\%$.⁴⁴ Co-sensitization increase the J_{sc} as well as V_{oc} because of enhancement of light harvesting ability and suppression of charge recombination. Chen and co-workers reported co-sensitization of porphyrin **HD18** with **PT-C6** which displayed η value of 10.1%.⁴⁵

Functionalization of porphyrin at β -position provide a new way to synthesize β -functionalized porphyrin dyes for DSSCs.⁴⁶⁻⁵³ β -Substituent have better electronic communication with porphyrin π -system which can lead superior light harvesting ability. β -Functionalized porphyrin dyes (**GD1**, **GD2** and **Zn-1**) were reported for DSSC applications with η -value of 5-7%.^{46,47} Kim and co-workers prepared two β -push-pull porphyrins namely **tda-1b-d-Zn** and **tda-2b-bd-Zn** with a higher PCE of 7.47% and 5.91%, respectively.⁴⁸ With suitable β -functionalization of porphyrins having strong electron donating and acceptor groups can modulate the optical and electronic properties which further improve the performance of porphyrin sensitizers.^{49,50} β -formylation or bromination of porphyrins are of special interest due to their easy transformation in several other functional groups.⁵¹⁻⁵³ β -Bromosubstituted porphyrins can be functionalized by various donor groups *via* coupling reactions whereas β -formyl group can also be converted into different acceptor groups e.g. carboxylic acid or cyanoacetic acid groups.⁵⁴⁻⁵⁹

To improve the efficiency of β -substituted porphyrins for DSSC, herein, we have synthesized three β -substituted push-pull Zn(II) porphyrin dyes by varying the substituents at *meso*- and β -positions as shown in figure 1. β -monoformylporphyrins were utilized as the precursors for the targeted porphyrin dyes in which formyl group undergo Knoevenagel condensation with cyanoacetic acid to introduce cyano-carboxylic acid as the acceptor group. Bulky groups such as *tert*-butyl and mesityl groups were introduced at *meso* position to prevent the dye aggregation of porphyrin molecules at TiO_2 surface and also provide an effective shielding to electron recombination with the electrolyte. Zn mesitylporphyrinic dye was further co-sensitized with N719 organic dye to improve the power conversion efficiency for DSSC. These porphyrin molecules were synthesized in good yields and characterized by UV-Vis., Fluorescence, ¹H-NMR and MALDI-MS spectroscopic techniques and elemental analysis.

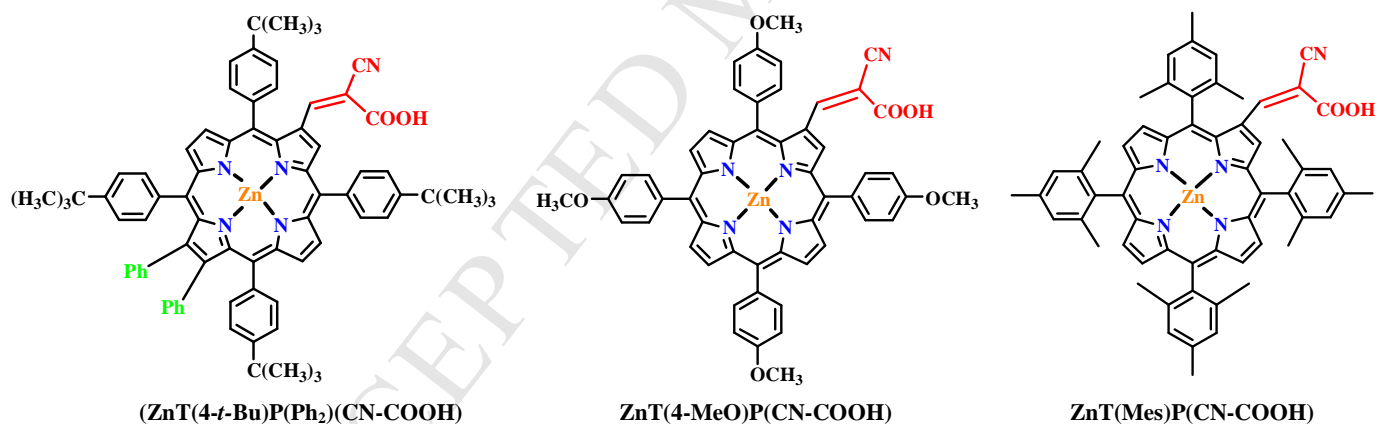


Figure1 Molecular structures of synthesized Zn(II) porphyrin dyes.

2. Experimental Section

2.1 Material

Pyrrole, propionic acid, piperidine, *p*-chloroanil, $Cu(OAc)_2 \cdot H_2O$ and $Zn(OAc)_2 \cdot 2H_2O$ were taken from HiMedia, India and N-Bromosuccinimide, cyanoacetic acid, sodium hydroxide, $BF_3 \cdot OEt_2$ were taken from SRL, India and used as received. $PhB(OH)_2$, 4-*tert*-butylbenzaldehyde and mesityldehyde were purchased from Alfa Aesar. 4-Methoxybenzaldehyde and $Pd(PPh_3)_4$ were taken from Sigma Aldrich and used without further purification. DMF and K_2CO_3 were received from Rankem. $POCl_3$ was taken from Thomas Baker. All solvents used in this work were distilled and then used. Column chromatography was carried on silica gel (Rankem laboratory, 100-200 mesh). $TBAPF_6$ was recrystallized twice with ethanol. Dry CH_2Cl_2 used in CV analysis was distilled twice with P_2O_5 and third time from CaH_2 .

2.2 Instrumentation and methods

Optical absorption spectra were recorded in dry CH_2Cl_2 using an Agilent Cary 100 spectrophotometer using a pair of quartz cells of 3.5 mL volume and 10 mm path length and fluorescence spectra were recorded using a Hitachi F-4600 spectrofluorometer using a quartz cell of 10 mm path length. ^1H NMR and ^{13}C NMR spectra were recorded using JEOL ECX 400 MHz spectrometer using $\text{DMSO}-d_6$ and CDCl_3 as solvents. Mass spectra were measured using a Bruker Ultraflex-treme-TN MALDI-TOF-MS spectrometer using HABA (2-(4'-hydroxybenzeneazo)benzoic acid) as matrix. Electrochemical measurements were carried out using CH instrument (CH 620E). A three electrode assembly used was consist of a platinum working electrode, Ag/AgCl as a reference electrode and a Pt-wire as a counter electrode. The concentration of all compounds was maintained at 1 mM. All measurements were performed in triple distilled CH_2Cl_2 containing 0.1M TBAPF_6 as supporting electrolyte, which was degassed by argon gas purging.

2.3 The fabrication of DSSCs

The dye-sensitized TiO_2 film was used as a photoanode in the solar cell and Pt foil used as counter electrode. Fluorine-doped SnO_2 glass (TEC-15, 2.2 mm thickness, Solaronix) was used for transparent conducting electrodes. Both the substrate was first cleaned in an ultrasonic bath using a detergent solution, acetone and ethanol, respectively (each step was 20 min long). The FTO glass plates were immersed into a 40 mM aqueous TiCl_4 solution at 70 °C for 30 min and washed with water and ethanol and then FTO plates were sintered at 500 °C for 30 min. A 9-10 μm thick layer of 20 nm sized TiO_2 particles deposited on FTO and sintered and were gradually heated under air flow at 325 °C for 5 min, at 375 °C for 5 min, at 450 °C for 15 min, and 500 °C for 15 min. Then 4 μm thick layer of 400 nm scattering layer was deposited over the 400 nm sized TiO_2 particles and gradually heated under air flow condition at 325 °C for 5 min, at 375 °C for 5 min, at 450 °C for 15 min, and 500 °C for 15 min. The electrodes were again immersed into a 40 mM TiCl_4 solution at 70°C for 30 minutes and washed with water and ethanol and sintered at 500°C. After cooling to room temperature, FTO plates are heated at 70°C and electrodes were then immersed in a 0.1 mM of porphyrin sensitizer in DMF/MeOH (volume ratio: 4:1) solutions and the dye solution contains 0.4mM CDCA (Solaronix, Switzerland) as an additive. Then the photoanodes underwent dipping condition for 20 h under dark conditions at a room temperature. After dye loading, photoanodes were washed with EtOH and dried by air flow. The co-sensitization was carried out by dipping porphyrin sensitized $(\text{ZnT}(\text{Mes})\text{P}(\text{CN-COOH})\text{TiO}_2$ in 0.5 mM N719 dye in ethanol for 2 h. The same experiment was repeated for 0.5 mM N719 dye alone. Finally electrolyte (AN-50, Solarix, Switzerland) solution was introduced into the space between the photoanodes and Pt sheet counter electrode.

2.4 Synthesis of Zn(II) Porphyrin dyes

2.4.1 Synthesis of 2'-Cyano-12,13-diphenyl-3'-(2-(5,10,15,20-meso-tetra-(4-tertiarybutylphenyl)PorphyrinatoZinc(II)yl)acrylic acid (ZnT(II)(4-*t*-Bu)P(Ph₂)(CN-COOH)):

$\text{H}_2\text{T}(4\text{-}t\text{-Bu})\text{P}$: 18.0 mL of Propionic acid was taken in a 100 mL round-bottom (RB) flask and warmed to about 10 minutes. To this, 0.5 mL (3 mmol) of 4-*t*-butylbenzaldehyde and 0.2 mL (3 mmol) pyrrole were added and then refluxed at 90 °C for 90 minutes. The reaction mixture was cooled to room temperature and filtered using G-4 sintered crucible washed and thoroughly with MeOH to remove polypyrrolic impurities. The compound was purified through silica gel column chromatography using chloroform as an eluent. The solvent was evaporated using rotary evaporator and the compound was recrystallized using $\text{CHCl}_3/\text{MeOH}$. The yield was found to be 16% (100 mg). UV-Vis. (CH_2Cl_2 , λ_{max} in nm): 420, 517, 554, 590, 648. ^1H NMR (CDCl_3 , 400 MHz): δ (ppm) 8.87 (s, 8H, β -pyrrole-Ph), 8.15(d, 8H, $J = 8$ Hz, *ortho*-Ph), 7.76(d, 8H, $J = 8$ Hz, *meta*-Ph), 1.61(s, 36H, *t*-Bu-H), -2.74 (s, 2H, -NH proton). Elemental analysis calcd. for $\text{C}_{60}\text{H}_{62}\text{N}_4$: C, 85.88; H, 7.45; N, 6.68% and found C, 85.15; H, 6.22; N, 7.75%.

$\text{Cu}(\text{II})\text{T}(4\text{-}t\text{-Bu})\text{P}$: 100 mg (0.12 mmol) of $\text{H}_2\text{T}(4\text{-}t\text{-Bu})\text{P}$ was dissolved in 15 mL of CHCl_3 , $\text{Cu}(\text{OAc})_2 \cdot \text{H}_2\text{O}$ (0.240 mg, 10 eq.) in 3.0 mL of MeOH was added to this porphyrin solution in CHCl_3 and refluxed for 30 minutes. After completion, the reaction mixture was washed two times with water to remove excess of Cu metal salt and the organic layer was separated with CHCl_3 . The crude porphyrin was purified by silica gel column chromatography using CHCl_3 as eluent and recrystallized using $\text{CHCl}_3/\text{MeOH}$. The yield of the product was found to be 90 % (95 mg). UV-Vis. (CH_2Cl_2 , λ_{max} in nm): 412, 540. Elemental analysis calcd. for $\text{C}_{60}\text{H}_{60}\text{N}_4\text{Cu}$: C, 80.01; H, 6.71; N, 6.22% and found C, 80.86; H, 6.27; N, 6.31%.

$\text{H}_2\text{T}(4\text{-}t\text{-Bu})\text{P}(\text{CHO})$: A 250 mL round bottom flask equipped with condenser, drying tube and thermometer was charged with DMF (1.0 mL) and POCl_3 (0.9 mL) at 0 °C and stirred for 15 minutes at room temperature until a golden-yellowish liquid was formed which indicates the formation of Vilsmeier-complex. 90 mg (0.10 mmol) $\text{CuT}(4\text{-}t\text{-Bu})\text{P}$ was diluted with a 15.0 mL of 1,2-dichloroethane under argon atmosphere. This porphyrinic solution was then added to the Vilsmeier-complex and refluxed for 7 h at 80 °C. After that the reaction mixture was cooled at room temperature for overnight. Then, 2.0 mL conc. H_2SO_4 was added to the reaction mixture and stirred for 10 minutes in ice bath. It was then neutralized with ice cold aqueous solution of NaOH (5.0 g in 100 mL distilled water). Then the reaction mixture was transferred to the separating funnel and CHCl_3 was added. The reaction mixture was washed with water until green color disappeared followed by washing with 20% aqueous solution of NaHCO_3 (2×100 mL). The organic layer was separated and dried over anhydrous sodium sulphate. The solvent was evaporated using rotary evaporator and the crude porphyrin was purified by column chromatography using CHCl_3 as eluent. The yield of the product was found to be 80% (70 mg). UV-Vis. (CH_2Cl_2 , λ_{max} in nm): 434, 539, 581, 606, 681. ^1H NMR (CDCl_3 , 400 MHz): δ (ppm) 9.45 (s, 1H, -CHO proton), 9.25 (s, 1H, β -pyrrole-H) 8.93-8.88 (m, 4H,

β -pyrrole-H), 8.80 (t, 2H, $J = 4.8$ Hz, β -pyrrole-H), 8.18-8.12 (m, 8H, *ortho*-PhH), 7.80-7.76 (m, 8H, *meta*-PhH), 1.61-1.60 (m, 36H, *t*-Bu-H), -2.50 (s, 2H, -NH proton). Elemental analysis calcd. for $C_{61}H_{62}N_4O$: C, 84.49; H, 7.21; N, 6.46% and found C, 84.41; H, 6.51; N, 6.47%.

$H_2T(4-t-Bu)P(Br_2)(CHO)$: In a 100 mL RB flask, $H_2T(4-t-Bu)P(CHO)$ (150 mg, 0.172 mmol) was taken in 40 mL of $CHCl_3$. To this solution, NBS (76 mg, 2.5 eq.) was added. The flask was covered with aluminum foil to protect the mixture from light and allowed to reflux for 24 h at 75 °C. The solvent was removed by rotary evaporation and the crude product was purified with column chromatography using 1:1 $CHCl_3$ /Hexane as an eluent. The yield of the product was found to be 50% (90 mg). UV-Vis. (CH_2Cl_2 , λ_{max} in nm): 441(5.16), 538(3.92), 687(3.75). 1H NMR ($CDCl_3$, 400 MHz): δ (ppm) 9.34 (s, 1H, -CHO proton), 9.16 (s, 1H, β -pyrrole-H), 8.94-8.85 (m, 4H, β -pyrrole-H), 8.20-8.09 (m, 8H, *ortho*-PhH), 7.83-7.79 (m, 8H, *meta*-PhH), 1.60-1.61 (m, 36H, *t*-Bu-H), -2.62 (s, 2H, -NH proton). MALDI-TOF-MS: m/z 1022.65 for $[M]^+$ (calcd. 1022.31). Elemental analysis calcd. for $C_{61}H_{60}Br_2N_4O$: C, 71.48; H, 5.90; N, 5.47% and found C, 74.12; H, 5.80; N, 5.67%. ^{13}C NMR (100 MHz, $CDCl_3$): δ (ppm) 188.8, 186.6, 152.8, 152.5, 152.2, 152.1, 151.9, 151.8, 151.3, 149.2, 148.2, 141.1, 140.8, 139.5, 139.2, 139.0, 138.1, 138.1, 138.0, 137.7, 137.6, 137.3, 136.7, 135.8, 135.6, 135.3, 135.2, 130.0, 129.7, 129.2, 129.1, 125.1, 124.8, 124.7, 124.6, 124.5, 124.2, 123.2, 122.9, 122.1, 120.7, 120.6, 120.5, 120.3, 120.2, 35.0, 31.7, 22.7, 14.7.

$H_2T(4-t-Bu)P(Ph_2)(CHO)$: The two-neck round-bottom flask (100 mL) containing distilled toluene (20 mL) was charged with $(H_2T(4-t-Bu)(CHO)Br_2)$ (50 mg, 0.048 mmol) and purged with argon gas. Then phenyl boronic acid (46 mg, 0.384 mmol, 8 eq.), K_2CO_3 (105 mg, 0.768 mmol, 16 eq.), $Pd(PPh_3)_4$ (12 mg, 20 mol %) were added and purged again with argon for 15 minutes. The reaction mixture was refluxed for 6 h at 100°C under inert atmosphere. After completion of the reaction, the solvent was evaporated under reduced pressure using rotary evaporator. The resulting residue was dissolved in minimum amount of $CHCl_3$ and washed with saturated aqueous $NaHCO_3$ solution followed by 30% aqueous $NaCl$ solution. The organic layer was separated and dried over anhydrous Na_2SO_4 . Solvent was evaporated using rotary evaporator. The crude porphyrin was purified by column chromatography using $CHCl_3$. The yield was found to be 50% (26 mg). UV-Vis. (CH_2Cl_2 , λ_{max} in nm): 443, 536, 682. 1H NMR ($CDCl_3$, 400 MHz): δ (ppm) 9.39 (s, 1H, -CHO proton), 9.27 (s, 1H, β -pyrrole-H), 8.79-8.75 (m, 2H, β -pyrrole-H), 8.61 (d, 2H, $J = 4$ Hz, β -pyrrole-H), 8.20 (d, 2H, $J = 8$ Hz, *ortho*-PhH), 8.16 (d, 2H, $J = 8.4$ Hz, *ortho*-PhH), 7.81-7.72 (m, 8H, *ortho* and *meta*-PhH), 7.26-7.21 (m, 4H, *meta*-PhH), 6.91-6.88 (m, 4H, β -pyrrole-PhH), 6.85-6.80 (m, 6H, β -pyrrole-PhH), 1.62-1.59 (m, 36H, *t*-Bu-H), -2.21 (s, 2H, -NH proton). MALDI-TOF-MS: m/z 1019.365 for $[M + H]^+$ (calcd. 1018.55). Elemental analysis calcd. for $C_{73}H_{70}N_4O$: C, 86.01; H, 6.92; N, 5.50% and found C, 86.15; H, 6.91; N, 5.06%. ^{13}C NMR (100 MHz, $CDCl_3$): δ (ppm) 189.2, 149.6, 149.0, 139.9, 139.4, 139.2, 138.6, 138.4, 137.9, 137.2, 137.0, 136.0, 135.4, 135.2, 135.0, 132.5, 132.3, 131.5, 130.3, 130.1, 128.6, 126.5, 125.2, 124.9, 124.5, 124.0, 123.2, 122.9, 122.6, 122.0, 114.6, 35.0, 34.6, 33.9, 32.0, 31.7, 31.5, 29.8, 29.6, 29.5, 29.3, 29.0.

$Zn(II)T(4-t-Bu)P(Ph_2)(CHO)$: $H_2T(4-t-Bu)P(Ph_2)(CHO)$ (20 mg, 0.019 mmol) was dissolved in 10 mL of $CHCl_3$. To this solution, $Zn(OAc)_2 \cdot 2H_2O$ (43 mg, 10 eq.) in 1 mL of MeOH was added and reflux for 30 minutes. The reaction mixture was then washed twice with water to remove excess of zinc metal salt and then the organic layer was separated with $CHCl_3$ and dried over anhydrous sodium sulphate. The crude porphyrin was purified by column chromatography using $CHCl_3$ as eluent and the yield of the product was found to be 85% (18 mg). UV-Vis (CH_2Cl_2 , λ_{max} in nm): 440, 567, 608. Elemental analysis calcd. for $C_{73}H_{68}N_4OZn$: C, 80.98; H, 6.33; N, 5.17% and found C, 80.27; H, 6.73; N, 5.01%.

$Zn(II)T(4-t-Bu)P(Ph_2)(CN-COOH)$: $Zn(II)T(4-t-Bu)P(Ph_2)(CHO)$ (15 mg, 0.0138 mmol) was dissolved in 10 mL of distilled $CHCl_3$ in 100 mL RB flask. Cyanoacetic acid (12.5 mg, 10 eq.) in 1 mL of CH_3CN was added to this solution followed by drop wise addition of piperidine (0.01 mL) and the resultant reaction mixture was refluxed overnight at 80 °C. After that, the reaction mixture was washed with H_3PO_4 (2.00 M solution). The organic layer was separated with $CHCl_3$ and dried over sodium sulphate. The solvent was removed under vacuum and the crude porphyrin was purified by silica gel column chromatography using $CHCl_3$ -MeOH (9: 1) as eluent. The yield of the product was found to be 87% (13 mg). UV-Vis (CH_2Cl_2 , λ_{max} in nm): 447, 574, 628. 1H NMR ($DMSO-d_6$, 400 MHz): δ (ppm) 9.97 (s, 1H, -COOH), 9.38 (s, 1H, β -pyrrole), 8.69-8.57 (m, 2H, β -pyrrole-H), 8.42-8.36 (m, 2H, β -pyrrole-H), 8.08-7.92 (m, 11H, *ortho*, *meta*-PhH and 1-ethenyl-H), 7.76-7.70 (m, 4H, *meta*-PhH), 7.51 (d, 2H, $J = 7.2$ Hz, *meta*-PhH), 7.02 (d, 4H, $J = 6.4$ Hz, β -pyrrole-*ortho*-PhH), 6.81-6.68 (m, 6H, β -pyrrole-*meta* and *p*-PhH), 1.38-1.19 (m, 36H, *t*-Bu-H). MALDI-TOF-MS: m/z 1147.249 for $[M]^+$ (calcd. 1147.59). Elemental analysis calcd. for $C_{73}H_{70}N_4O$: C, 79.39; H, 6.05; N, 6.09% and found C, 79.87; H, 6.42; N, 5.12%.

2.4.2 Synthesis of 2'-Cyano-3'-(2-5,10,15,20-meso-tetra(4-methoxyphenyl)PorphyrinatoZinc(II)acrylic acid ($Zn(II)T(4-MeO)P(CN-COOH)$):

$H_2T(4-MeO)P$: Synthetic procedure is similar to above reported Adler-Longo method. 16% yield. UV-Vis. (CH_2Cl_2 , λ_{max} in nm): 421(5.52), 518(4.09), 554(4.18), 596(3.60), 651(3.72). Elemental analysis calcd. for $C_{48}H_{38}N_4O_4$: C, 78.45; H, 5.21; N, 7.62% and found C, 78.26; H, 5.63; N, 5.10%.

Cu metallation of $H_2T(4-MeO)P$ and the formylation of $CuT(4-MeO)P$ were carried out using the above mentioned procedures.

$Cu(II)T(4-MeO)P$: 87% yield. UV-Vis. (CH_2Cl_2 , λ_{max} in nm): 417, 541, 577. Elemental analysis calcd. for $C_{48}H_{36}N_4O_4Cu$: C, 72.39; H, 4.56; N, 7.04% and found C, 72.36; H, 4.10; N, 5.41%.

$H_2T(4-MeO)P(CHO)$: The yield was found to be 70%. UV-Vis. (CH_2Cl_2 , λ_{max} in nm): 437(5.64), 531(4.34), 572(4.09), 606(3.89), 675(4.08). 1H NMR ($CDCl_3$, 400 MHz): δ (ppm) 9.41 (s, 1H, -CHO proton), 9.34 (s, 1H, β -pyrrole-H), 8.90 (m, 4H, β -pyrrole-H), 8.80 (t, 2H, $J = 5.6$ Hz, β -pyrrole-H), 8.14-8.10 (m, 8H, *ortho*-PhH), 7.30-7.27 (m, 8H, *meta*-PhH), 4.10-4.08 (m, 12H, -OCH₃ proton), -2.50 (s, 2H, -NH proton). MALDI-TOF-MS:

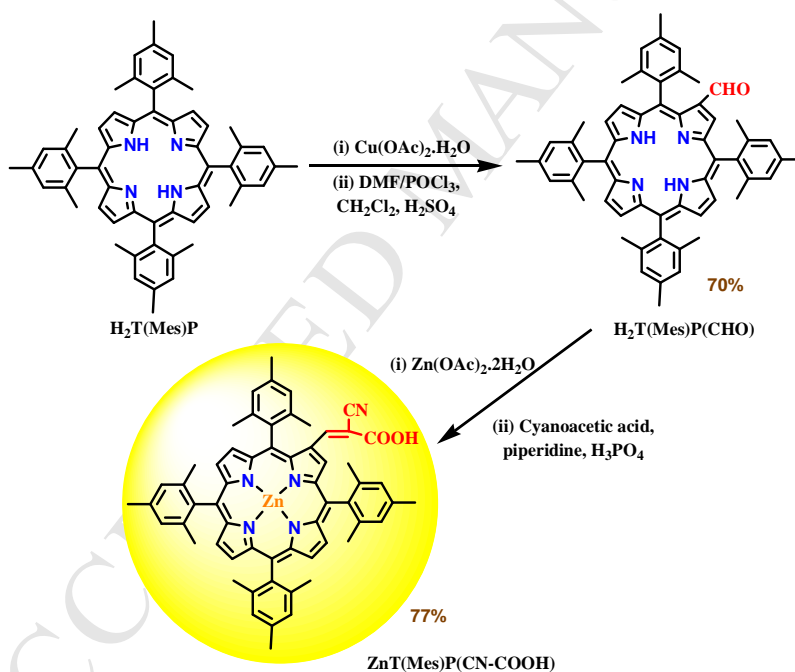
m/z 762.93 for $[M + H]^+$ (calcd. 762.28). Elemental analysis calcd. for $C_{49}H_{38}N_4O_5$: C, 77.15; H, 5.02; N, 7.34% and found C, 77.26; H, 5.19; N, 7.93%. ^{13}C NMR (100 MHz, $CDCl_3$): δ (ppm) 189.6, 160.4, 159.9, 159.7, 136.3, 136.0, 135.9, 135.8, 135.0, 134.4, 134.2, 122.5, 120.3, 120.0, 1119.8, 113.0, 112.5.

Zn(II)T(4-MeO)P(CHO): 80% (45 mg). UV-Vis. (CH_2Cl_2 , λ_{max} in nm): 437(5.30), 560(3.97), 605(3.86). 1H NMR ($CDCl_3$, 400 MHz): δ (ppm) 9.56 (s, 1H, -CHO proton), 9.41 (s, 1H, β -pyrrole-H), 8.97-8.93 (m, 6H, β -pyrrole-H), 8.16-8.07 (m, 8H, *ortho*-PhH), 7.33-7.21 (m, 8H, *meta*-PhH), 4.10-4.08 (m, 12H, MeO-proton). MALDI-TOF-MS: m/z 825.02 for $[M + H]^+$ (calcd. 825.20). Elemental analysis calcd. for $C_{49}H_{36}N_4O_5Zn$: C, 71.23; H, 4.39; N, 6.78% and found C, 71.56; H, 4.19; N, 6.06%. ^{13}C NMR (100 MHz, $CDCl_3$): δ (ppm) 190.3, 160.1, 159.0, 159.4, 152.2, 152.1, 152.0, 151.7, 151.1, 150.5, 147.7, 146.7, 141.6, 136.0, 135.8, 135.7, 135.7, 135.6, 135.5, 134.9, 134.7, 133.3, 133.0, 132.9, 132.7, 132.4, 123.4, 121.3, 121.0, 120.6, 121.7, 112.4, 55.7.

Zn(II)T(4-MeO)P(CN-COOH): The Knoevenagel condensation was carried out as mentioned above. The yield of the product was found to be 88% (38 mg). UV-Vis. (CH_2Cl_2 , λ_{max} in nm): 452(4.96), 568(3.92), 619(3.91). 1H NMR ($DMSO-d_6$, 400 MHz): δ (ppm) 9.44 (s, 1H, β -pyrrole-H) 8.82-8.74 (m, 6H, β -pyrrole-H), 8.10-7.93 (m, 9H, *ortho*-PhH and 1-ethenyl-H), 7.35-7.28 (m, 8H, *meta*-PhH), 4.03-4.01 (m, 12H, -OCH₃-proton). MALDI-TOF-MS: m/z 891.63 for $[M]^+$ (calcd. 891.20). Elemental analysis calcd. for $C_{52}H_{37}N_5O_6Zn$: C, 69.92; H, 4.17; N, 7.84% and found C, 69.86; H, 4.59; N, 7.90%. ^{13}C NMR (100 MHz, $DMSO-d_6$): δ (ppm) 160.2, 159.4, 159.3, 151.0, 150.8, 150.1, 142.1, 136.1, 135.7, 135.3, 135.2, 135.0, 134.8, 133.1, 132.7, 132.6, 132.5, 132.4, 132.3, 132.2, 120.8, 120.5, 113.4, 114.8, 79.7, 55.9, 34.0, 34.3, 33.7, 33.1, 32.0, 31.8, 31.2, 29.2.

2.4.3 Synthesis of 2'-Cyano-3'-(2-(5,10,15,20-meso-tetramesityl) Porphyrinato) Zinc(II)acrylic acid (Zn(II)T(Mes)P(CN-COOH)):

H₂T(Mes)P: Tetramesitylporphyrin was synthesized according to reported Lindsey method.⁶² Yield 29%. UV-Vis. (CH_2Cl_2 , λ_{max} in nm): 418(5.63), 514(4.20), 548(3.57), 594(3.70), 648(3.48). 1H NMR ($CDCl_3$, 400 MHz): δ (ppm) 8.62 (s, 8H, β -pyrrole-H), 1.85 (s, 24H, *ortho*-ArCH₃), 1.62 (s, 12H, *para*-ArCH₃), -2.51 (s, 2H, -NH proton). Elemental analysis calcd. for $C_{56}H_{54}N_4$: C, 85.89; H, 6.95; N, 7.15% and found C, 85.61; H, 6.38; N, 7.91%.



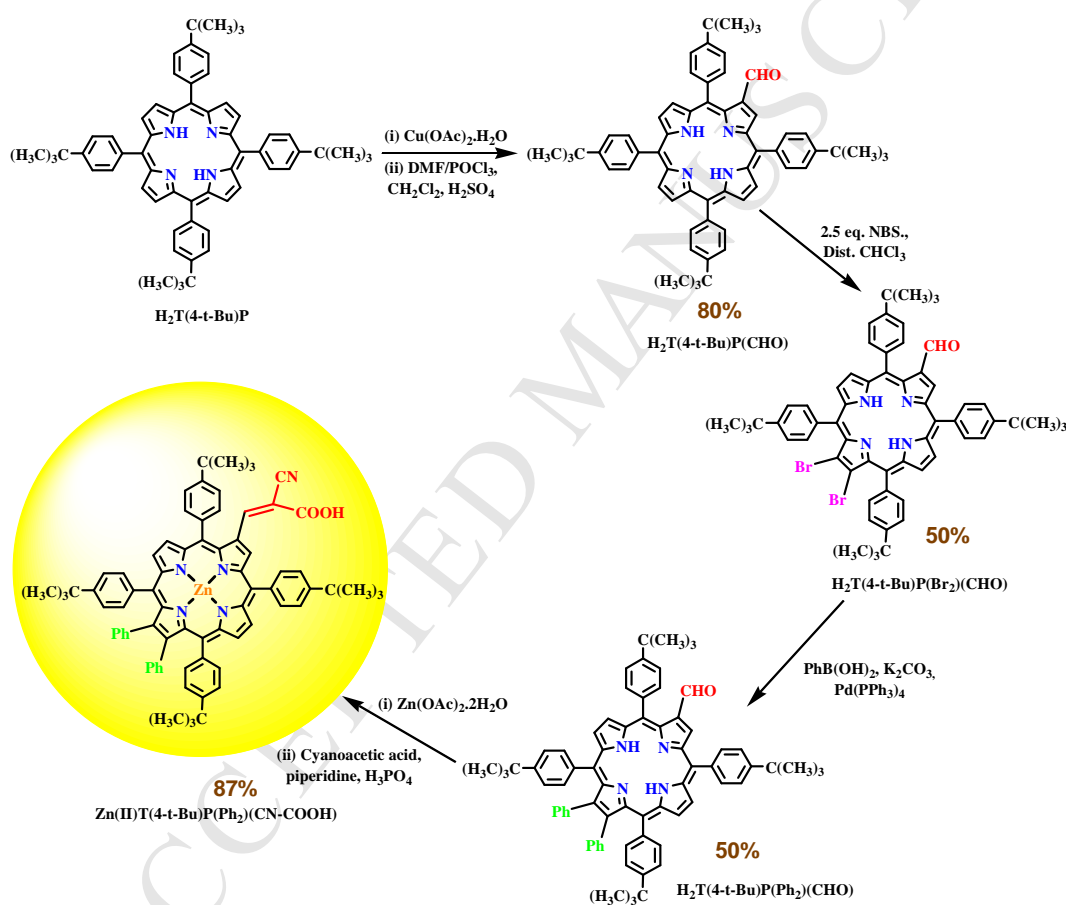
Scheme 1: Synthetic Route of ZnT(Mes)P(CN-COOH) dye

Cu(II)T(Mes)P: Yield (80 mg). UV-Vis. (CH_2Cl_2 , λ_{max} in nm): 415, 539. Elemental analysis calcd. for $C_{56}H_{52}N_4Cu$: C, 79.64; H, 6.21; N, 6.63% and found C, 79.50; H, 6.13; N, 6.82%.

H₂T(Mes)P(CHO): The formylation was performed as mentioned above. The yield was found to be 70% (60 mg). UV-Vis. (CH_2Cl_2 , λ_{max} in nm): 437, 531, 572, 606, 675. 1H NMR ($CDCl_3$, 400 MHz): δ (ppm) 9.41 (s, 1H, -CHO proton), 9.30 (s, 1H, β -pyrrole-H) 8.68-8.57 (m, 6H, β -pyrrole-H), 7.29-7.27 (m, 6H, *meta*-PhH), 7.26-7.25 (m, 2H, *meta*-PhH), 2.63 (d, 12H, $J = 3.6$ Hz, *para*-ArCH₃ proton), 1.89 (d, 18H, $J = 7.6$ Hz, *meta*-ArCH₃ proton), 1.83 (s, 6H, *meta*-ArCH₃ proton), -2.21 (s, 2H, -NH proton). MALDI-TOF-MS: m/z 811.23 for $[M + H]^+$ (calcd. 811.43). Elemental analysis calcd. for $C_{57}H_{54}N_4O$: C, 84.41; H, 6.71; N, 6.91% and found C, 84.07; H, 6.21; N, 6.32%. ^{13}C NMR (100 MHz, $CDCl_3$): δ (ppm) 190.4, 139.8, 139.5, 139.4, 139.3, 138.0, 137.9, 137.8, 137.6, 129.1, 128.56, 128.48, 128.3, 128.0, 127.9, 125.4, 120.6, 118.2, 117.9, 117.8, 32.0, 31.7, 30.43, 30.3, 29.8, 29.6, 29.5, 29.4, 29.2.

Zn(II)T(Mes)P(CHO): 88%. UV-Vis. (CH_2Cl_2 , λ_{max} in nm): 436(5.53), 562(4.23), 604(4.08). ^1H NMR (CDCl_3 , 400 MHz): δ (ppm) 9.43 (s, 1H, -CHO proton), 9.37 (s, 1H, β -pyrrole-H), 8.69-8.62 (m, 6H, β -pyrrole-H), 7.26-7.23 (m, 8H, *meta*-PhH), 2.61 (d, 12H, $J = 4.8$ Hz, *para*-ArCH₃ proton), 1.85 (d, 18H, $J = 7.2$ Hz, *meta*-ArCH₃ proton), 1.81 (s, 6H, *meta*-ArCH₃ proton). MALDI-TOF-MS: m/z 873.27 for $[\text{M} + \text{H}]^+$ (calcd. 873.34). Elemental analysis calcd. for $\text{C}_{57}\text{H}_{52}\text{N}_4\text{OZn}$: C, 78.29; H, 5.99; N, 6.41% and found C, 78.48; H, 6.09; N, 6.26%. ^{13}C NMR (100 MHz, CDCl_3): δ (ppm) 191.3, 151.5, 151.1, 150.4, 155.6, 139.7, 139.5, 139.4, 139.3, 139.2, 138.9, 137.8, 137.7, 135.0, 132.3, 132.2, 131.4, 128.4, 127.9, 118.5, 116.1, 114.3, 45.0, 34.9, 34.0, 32.1, 31.8, 31.2.

ZnT(Mes)P(CN-COOH): The synthetic procedure of this compound is same as previously described. 77% (25 mg). UV-Vis. (CH_2Cl_2 , λ_{max} in nm): 453(5.53), 562(4.23), 612(3.90). ^1H NMR ($\text{DMSO}-d_6$, 400 MHz): δ (ppm) 8.99 (s, 1H, β -pyrrole-H) 8.44-8.40 (m, 6H, β -pyrrole-H), 7.90 (s, 1H, 1-ethenyl-H), 7.23-7.21 (m, 8H, *meta*-PhH), 2.45 (d, 12H, $J = 6.4$ Hz, *para*-ArCH₃-proton), 1.74 (d, 18H, $J = 4$ Hz, *meta*-ArCH₃-proton), 1.68 (s, 12H, *meta*-ArCH₃-proton). MALDI-TOF-MS: m/z 940.28 for $[\text{M} + \text{H}]^+$ (calcd. 940.35). Elemental analysis calcd. for $\text{C}_{60}\text{H}_{53}\text{N}_5\text{O}_2\text{Zn}$: C, 76.54; H, 5.67; N, 7.44% and found C, 76.98; H, 5.17; N, 7.31%. ^{13}C NMR (100 MHz, $\text{DMSO}-d_6$): δ (ppm) 163.7, 150.6, 150.48, 150.44, 150.36, 150.0, 159.4, 139.3, 139.2, 139.0, 138.9, 138.88, 137.5, 132.0, 131.7, 131.6, 131.59, 131.3, 128.7, 128.2, 128.16, 128.0, 118.2, 117.6, 79.7, 34.7, 29.6.



3. Result and discussion

3.1 Synthesis

We designed and synthesized three new β -functionalized porphyrins by varying the *meso*-position with bulky groups (*t*-butyl and mesityl) and incorporating electron-donating Ph groups at β -position of porphyrin. The targeted Zn(II) Porphyrins were synthesized by facile routes having high yields. The synthetic routes for Zn(II)T(Mes)P(CN-COOH) and Zn(II)T(4-*t*-Bu)P(Ph₂)(CN-COOH) dyes were shown in scheme 1 and 2. The synthetic route for Zn(II)T(4-MeO)P(CN-COOH) was shown in ESI (scheme S1). Firstly, *meso*-tetraarylporphyrins were synthesized by Adler-Longo and Lindsey method which further underwent formylation to synthesize free-base monoformyltetraarylporphyrins.^{60,62} The formylation and Cu/Zn

metallation have been carried out according to reported procedure in good yields (70-90%).^{27,61,55} To obtain the target porphyrinic dyes, Zn(II) monoformyl porphyrins were directly converted into targeted dyes by condensation with cyanoacetic acid.⁴⁶ But, in case of *t*-Bu-Ph porphyrinic dyes, regioselective dibromination and Suzuki coupling reaction with phenyl boronic acid were carried out in order to append an electron-donating phenyl substituent on β -pyrrolic position of porphyrin core⁵² and then it further proceeded for Zn metallation and Knoevenagel condensation to obtain desired porphyrin dye.⁴⁶ All dyes were synthesized in very good yields and characterized by UV-Vis, Fluorescence, ¹H-NMR, ¹³C-NMR and MALDI-TOF-MS spectroscopic techniques. The photophysical and electrochemical measurement have also been performed for all these Zn(II) porphyrin dyes.

3.2 Electronic spectral and NMR studies

The UV-Vis absorption spectra of all porphyrin dyes and their precursors were recorded in CH₂Cl₂ at 298 K. The typical strong Soret and Q bands were observed due to $\pi - \pi^*$ transitions of conjugated porphyrin systems. The spectral data of all porphyrins are listed in Table 1. The monoformyl porphyrins H₂T(4-MeO)P(CHO), H₂T(Mes)P(CHO) and H₂T(4-*t*-Bu)P(CHO) exhibited 10-12 nm shift in the absorption band from their parent unsubstituted porphyrin.²⁷

Table 1. UV-Visible and Emission data of all synthesized porphyrin molecules in CH₂Cl₂ at 298 K.

Porphyrins	B band, λ_{\max} , nm	Emission, λ_{em} , nm	Quantum Yield, ϕ_r	Life Time, τ (ns)
H ₂ T(4-MeO)P	421(5.52), 518(4.09), 554(4.18), (3.60), 651(3.72)	660	0.1956	8.23
H ₂ T(4-MeO)P(CHO)	437(5.64), 531(4.34), 572(4.09), 606(3.89), 675(4.08)	693	0.0675	4.17
ZnT(4-MeO)P(CHO)	437(5.30), 560(3.97), 605(3.86)	637	0.0082	0.84
ZnT(4-MeO)P(CN-COOH)	452(4.96), 568(3.92), 619(3.91)	682	0.0055	1.73
H ₂ T(Mes)P	418(5.63)(4.20), 548(3.57), 594(3.70), 648(3.48)	658	0.1362	9.65
H ₂ T(Mes)P(CHO)	433, 310, 348, 526, 569, 606, 663	678	0.0919	7.49
ZnT(Mes)P(CHO)	436(5.53), (4.23), 604(4.08)	622	0.0162	1.58
ZnT(Mes)P(CN-COOH)	399(sh)(4.51), 453(4.89), 562(3.89), 612(3.90)	666	0.0114	1.16
H ₂ T(4- <i>t</i> -Bu)P	420, 517, 554, 590, 648	688	0.2384	7.67
H ₂ T(4- <i>t</i> -Bu)P(CHO)	434(5.57), (4.33), 573(4.07), 606(3.96), 665(4.07)	688	0.0786	5.72
H ₂ T(4- <i>t</i> -Bu)P(CHO)(Br ₂)	441(5.16), 538(3.92), 687(3.75)	622, 731	0.0008	0.87
H ₂ T(4- <i>t</i> -Bu)P(CHO)(Ph ₂)	443, 682	723	0.0372	*
ZnT(4- <i>t</i> -Bu)P(Ph ₂)(CN-COOH)	447, 628	651	0.0032	0.74

*lifetime was too low to detect. ^aThe values in parentheses refer to log ϵ values, ϵ in dm³ mol⁻¹ cm⁻¹; sh = shoulder; error in quantum yield values 1–2%.

Figure 2a represents absorption spectra of target Zn(II) porphyrin dyes. All synthesized porphyrin dyes exhibited broad Soret band in the range of 445–455 nm and moderate Q bands in the range of 560–630 nm. Porphyrin dyes having mesityl and methoxy groups at *meso*-position showed marginal red-shift (7–8 nm) in Soret band as compared to dyes having phenyl group at β -pyrrole position. The synthesized porphyrins were also characterized by fluorescence spectroscopy to investigate the effect of different groups on porphyrin moiety.

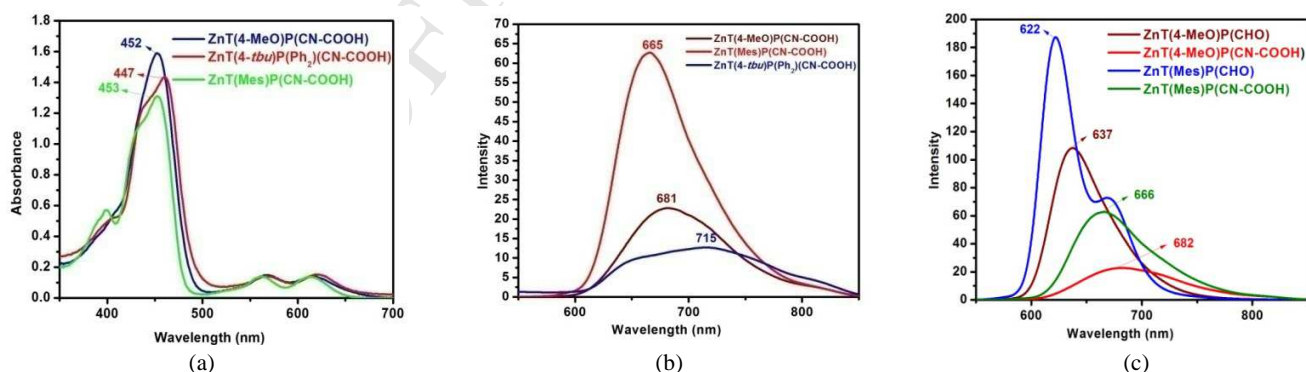


Figure 2: (a) UV-Vis absorption spectra of Zn(II) Porphyrin dyes. (b) Fluorescence Spectra of compound all Zn(II) Porphyrin dyes. (c) Comparison of Fluorescence Spectra of Zn(4-MeO)P(CHO), Zn(Mes)P(CHO) to their corresponding dyes ZnT(4-MeO)P(CN-COOH) and ZnT(Mes)P(CN-COOH) in CH₂Cl₂ at 298K.

The emission spectra of all three Zn porphyrin dyes in CH_2Cl_2 at 298 K were presented in fig. 2b and their emission data is illustrated in table 1. ZnT(4-MeO)P(CN-COOH), ZnT(4-*t*-Bu)P(Ph₂)(CN-COOH) and ZnT(Mes)P(CN-COOH) dyes exhibited broad emission spectral features. Fluorescence quenching was observed for all Zn(II) porphyrin dyes compared to their parent Zn(II) monoformyl porphyrins as shown in fig 2c, which indicates an efficient charge transfer from donor to acceptor. Figures S1-S6 in the ESI represent the UV-Vis and fluorescence spectral features of all synthesized porphyrins. The Quantum yield decreases in this order: ZnT(Mes)P(CN-COOH) > ZnT(4-MeO)P(CN-COOH) > ZnT(4-*t*-Bu)P(Ph₂)(CN-COOH) which suggest an efficient charge-transfer in ZnT(4-*t*-Bu)P(Ph₂)(CN-COOH) as compared to other two dyes. The ZnT(4-*t*-Bu)P(Br₂)(CHO) exhibited fluorescence quenching and led to the decrement in the quantum yield due to the heavy atom effect of the bromo substituent at β -position.

Quantum yields (ϕ) were calculated by using the equation given below

$$\phi_{\text{sample}} = (\phi_{\text{ref}} \times A_{\text{sample}} \times I_{\text{ref}}) / (A_{\text{ref}} \times I_{\text{sample}})$$

¹H-NMR spectra of Zn porphyrin dyes and their precursor molecules were recorded in DMSO-*d*₆ and CDCl₃, respectively at 298 K and shown in the ESI (figure S7-14). The key feature of proton NMR of all mono-formyl porphyrin is -CHO, β -pyrrole, *meso*-phenyl and imino protons. All porphyrins exhibited their characteristic signals for mesityl CH₃-OCH₃ and *tert*-butyl protons. The characteristic signal of formyl group and adjacent β -pyrrole-H appeared in the range of 9.15-9.50 ppm whereas other β -pyrrole-H signals were found in the range of 8.57-8.95 ppm. The signal of formyl proton for H₂T(4-*t*-Bu)P(CHO) showed downfield shift by 0.04-0.06 ppm relative to other mono-formyl porphyrins. The β -pyrrole proton of H₂T(4-*t*-Bu)P(Ph₂)(CHO) and H₂T(Mes)P(CHO) exhibited upfield shift than other porphyrins. The *ortho*-, *meta*-PhH and imino- proton signals of H₂T(4-*t*-Bu)P(Br₂)(CHO) and H₂T(4-*t*-Bu)P(Ph₂)(CHO) exhibited downfielded and upfielded shift, respectively as compared to other porphyrins due to different electronic nature of bromo and phenyl group. The β -pyrrole PhH of H₂T(4-*t*-Bu)P(Ph₂)(CHO) were found in the range of 6.80-6.90 ppm. All Zn porphyrin dyes show one proton signals for β -pyrrole-H adjacent to cyanoacetic acid group in the range of 8.91-9.38 ppm whereas other β -pyrrole-H signals were found in the range of 8.35-8.85 ppm. The ethenyl protons of Zn porphyrin dyes were generally featured with *ortho*-phenyl protons (PhH) whereas the ethenyl proton of ZnT(Mes)P(CN-COOH) was found as a singlet at 7.90 ppm due to the absence of *ortho* protons. The -COOH proton of cyanoacetic acid group of ZnT(4-*t*-Bu)P(Ph₂)(CN-COOH) was appeared as a singlet at 9.97 ppm. The ¹³C-NMR spectra of newly synthesised porphyrins were recorded in DMSO-*d*₆ and CDCl₃ at 298 K (figures S17-24 in the ESI). However, the solubility of ZnT(4-*t*-Bu)P(Ph₂)(CN-COOH) was too poor in deuterated solvents (DMSO-*d*₆ and CDCl₃) to record the ¹³C NMR spectrum even at higher number of scans (upto 10000). The number and position of carbon signals in the spectra are in accordance with proposed structure of the corresponding porphyrins. The formyl carbon appeared around 190 ppm in parent monoformyl porphyrins and ethenyl carbon signal was found at 79 ppm in target Zn porphyrin dyes. The methoxy carbon signals were found at 55 ppm in methoxy porphyrins series. The porphyrin macrocycle signals appeared in the range of 110-160 ppm whereas alkyl carbon signals appeared in the range of 30-60 ppm in all synthesised porphyrins. The MALDI-TOF mass data were also recorded and shown in the ESI (figure S25-S33).

3.4 Electrochemical Redox properties

The electrochemical studies were performed for all porphyrins to examine the effect of substitutions on the porphyrin core. The electrochemical redox data of porphyrins were measured in CH_2Cl_2 containing 0.1M TBAPF₆ at 298 K and listed in table 2. The redox potentials of porphyrins can be affected by the variation of *meso*- and β -substituent and with different metal ions.

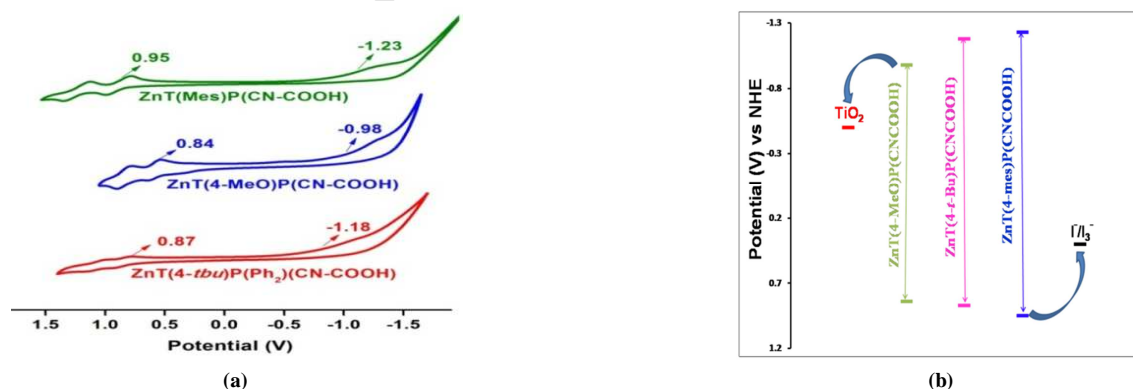


Fig. 3 (a) CV of Zn(II) porphyrin Dyes in CH_2Cl_2 at 298 K and (b) Energy level diagram of dyes compared with the conduction band of TiO₂ and I⁻/I₃⁻ electrolyte.

Figure 3a represents the cyclic voltammograms (CVs) of all β -substituted Zn porphyrin dyes in CH_2Cl_2 at 298 K. The CV diagrams of all other porphyrins were shown in ESI (fig. S34). The first oxidation potential of all porphyrin molecules were found the range of 0.84 to 1.16 V whereas the

first reduction potential varied from -0.90 to -1.34 V. Free base tetraarylporphyrins show anodic shift in their first ring oxidation (0.02-0.16 V) and reduction potential as compared to H₂TPP. In case of H₂T(Mes)P(CHO), a dramatic cathodic shift in their first oxidation potential (0.07 V) and reduction potential (0.012 V) as compared to H₂T(Mes)P was observed whereas an opposite trend was observed for H₂T(4-*t*-Bu)P(CHO) as compared to H₂T(4-*t*-Bu)P. The first ring oxidation potential of H₂T(4-MeO)P(CHO) was unaltered as compared to H₂T(4-MeO)P whereas cathodic shift was observed for the first ring reduction potential.

Table 2. Cyclic Voltammetry Studies depicting Oxidation & Reduction Potentials of all the Synthesized Porphyrins in CH₂Cl₂ at 298 K.

Porphyrins	Oxidation (V)			Reduction (V)		$\Delta E_{1/2}$ (V)
	I	II	III	I	II	
H ₂ T(4-MeO)P	0.99	1.15	-	-1.05 ¹	-1.31 ^a	2.04
H ₂ T(4- <i>t</i> -bu)P	1.02	1.40	1.56 ^a	-1.17 ^a	-	2.19
H ₂ T(Mes)P	1.16	1.63	-	-1.14 ^a	-	2.30
H ₂ (4-MeO)P(CHO)	0.99	1.16	-	-1.08	-1.30 ^a	2.07
H ₂ T(4- <i>t</i> -bu)P(CHO)	1.05	1.27	1.51 ^a	-1.07	-1.29 ^a	2.11
H ₂ T(Mes)P(CHO)	1.09	1.63 ^a	-	-1.26 ^a	-	2.35
H ₂ T(4- <i>t</i> -bu)P(CHO)(Br ₂)	1.06	1.21	-	-0.90	-	1.97
ZnT(4-MeO)P(CHO)	0.87	1.16	-	-1.20	-	2.06
ZnT(Mes)P(CHO)	0.95	1.31	-	-1.34	-	2.29
ZnT(4-MeO)P(CN-COOH)	0.84	1.09	-	-0.98 ^a	-1.54 ^a	1.82
ZnT(4- <i>t</i> -bu)P(Ph ₂)(CN-COOH)	0.87	1.08	-	-1.18 ^a	-	2.05
ZnT(Mes)P(CN-COOH)	0.95	1.30	-	-1.23 ^a	-	2.18

Scan rate = 0.1 V/s. ^aData taken from DPV. ^b $\Delta E_{1/2} = E_{\text{oxd}} - E_{\text{red}}$. Pt working and Pt wire counter electrodes were used.

These Zn porphyrin dyes exhibited anodic shift in their first reduction and oxidation potential (0.03-0.11 V) as compared to ZnTPP whereas the first oxidation potential of ZnT(4-MeO)P(CN-COOH) has shown only marginal changes. Figure 3b depicted the HOMO-LUMO energy levels of Zn porphyrin dyes and compared with the conduction band of TiO₂ and the electrolyte I/I₃⁻. The result showed that the HOMO levels of all the dyes are sufficiently higher than the energy level of electrolyte (I/I₃⁻) which indicates that the oxidized sensitizers could be easily regenerated by the electrolyte. The LUMO levels of these dyes are significantly lower than the conduction band energy levels of TiO₂ which provides an efficient electron injection into the TiO₂ conduction band from the excited sensitizers. This shows the feasibility of electron transfer in DSSC.

3.5 Photovoltaic Studies

Dye-sensitized solar cells (DSSCs) were fabricated with β -substituted push pull Zn(II)-porphyrin-sensitized 12 μm thick TiO₂ photoanodes (0.16 cm²) assembled into standard sandwiched cells having Pt sheet as counter electrode. The space between the photoanodes is filled with iodide/triiodide electrolyte I/I₃⁻. The ZnT(Mes)P(CN-COOH) dye was co-sensitized with N719 organic dye and also studied for DSSC application. The photocurrent density-voltage (I-V characteristics) of synthesized Zn(II) porphyrin dyes are shown in figure 4a and the corresponding photovoltaic data under AM 1.5G solar light illumination (power 100 mW cm⁻²) with an active area of 0.16 cm², is listed in table 3. The data for commercial N719 dye under similar conditions is also added for comparison.

Table 3. Photovoltaic parameters of Zn(II) porphyrins under AM 1.5G sun illumination (power 100 mW cm²) with an active area of 0.16 cm²

Zn-Porphyrin dyes	V_{oc} (V)	J_{sc} (mA/cm ²)	FF (%)	η (%)
ZnT(Mes)P(CN-COOH)	0.575	7.8	70	3.13
ZnT(4-MeO)P(CN-COOH)	0.570	5.7	70	2.27
ZnT(4- <i>t</i> -Bu)P(Ph ₂)(CN-COOH)	0.58	4.3	69	1.72
ZnT(Mes)P(CN-COOH)(N719 dye)	0.63	11.8	72	5.35
STD-N719 (ref)	0.61	6.7	68	2.77

The overall power conversion efficiencies (PCE) lie in the range of 1.72-5.35%, follows the order as ZnT(4-*t*-Bu)P(CN-COOH) ($\eta = 1.72\%$) < ZnT(4-MeO)P(CN-COOH) ($\eta = 2.27\%$) < ZnT(Mes)P(CN-COOH) ($\eta = 3.13\%$) < ZnT(4-Mes)P(CN-COOH)(N719 dye) ($\eta = 5.35\%$). ZnT(Mes)P(CN-COOH) exhibited higher PCE efficiency as compared to ZnT(4-*t*-Bu)P(CN-COOH) and ZnT(Mes)P(CN-COOH) as dye aggregation has been effectively suppressed by mesityl group. Notably, the co-sensitization of ZnT(Mes)P(CN-COOH) with N719 dye enhanced the PCE efficiency upto 5.35%, with a J_{sc} of 11.8 mA cm⁻², a V_{oc} of 630 mV and a fill factor (FF) of 72%. N719 increase the device voltage which leads to high photo conversion efficiency for DSSCs. The incident photon-to-current conversion efficiency (IPCE) spectra were recorded as a function of incident wavelength using a Newport IPCE system as shown in figure 4b and 4c. These spectra slightly broader but follow the absorption spectra of the corresponding dyes where red shift seen in Soret and Q band absorption of Zn(II) porphyrin dyes in IPCE spectra. The broadness of IPCE spectra

demonstrate the better light harvesting ability of Zn porphyrin dyes. As shown in figure 4b, ZnT(Mes)P(CN-COOH) exhibited broader IPCE spectra as compared to other porphyrin dyes. Co-sensitized ZnT(Mes)P(CN-COOH) with N719 dye shows much broader IPCE spectrum in the range 400-700 nm as similar to Ru-dyes which suggests that co-sensitization of ZnT(Mes)P(CN-COOH) dye with N719 dye improve their light harvesting ability as well as their Power conversion efficiency (PCE) upto 5.35%. The broader the IPCE spectra, the greater the light harvesting ability of Zn porphyrin dyes and higher the PCE value as depicted in table 3. Bulky groups such as *tert*-butyl and mesityl groups present in ZnT(4-*t*-Bu)P(Ph)₂(CN-COOH) and ZnT(Mes)P(CN-COOH) suppressed the dye aggregation of these dyes at TiO₂ surface and also reduce the possibilities of charge recombination with the electrolyte that enhance the efficiency of DSSCs.

The IPCE spectra of co-sensitized ZnT(Mes)P(CN-COOH)(N719) porphyrin showed that the IPCE value of co-sensitized porphyrin dye is higher than ZnT(Mes)P(CN-COOH) and N719 dye with higher J_{sc} , V_{oc} , and FF of 72%, corresponding to overall conversion efficiency of 5.35%. The IPCE values for the dyes follow the order: ZnT(4-*t*-Bu)P(Ph)₂(CN-COOH) < ZnT(4-MeO)P(CN-COOH) < ZnT(Mes)P(CN-COOH) < co-sensitized ZnT(Mes)P(CN-COOH)(N719) which is in agreement with J_{sc} values obtained and the corresponding PCE values as shown in table 3. Further, the J-V curves under standard AM 1.5G illumination are in qualitative agreement with the photo-action spectra of these Zn(II) porphyrin dyes. Hence, the mesityl group prevents the dye aggregation and charge recombination. Further, the co-sensitization of N719 dye with Zn(II) porphyrin enhances the light harvesting capacity in visible region as shown figure 4c.

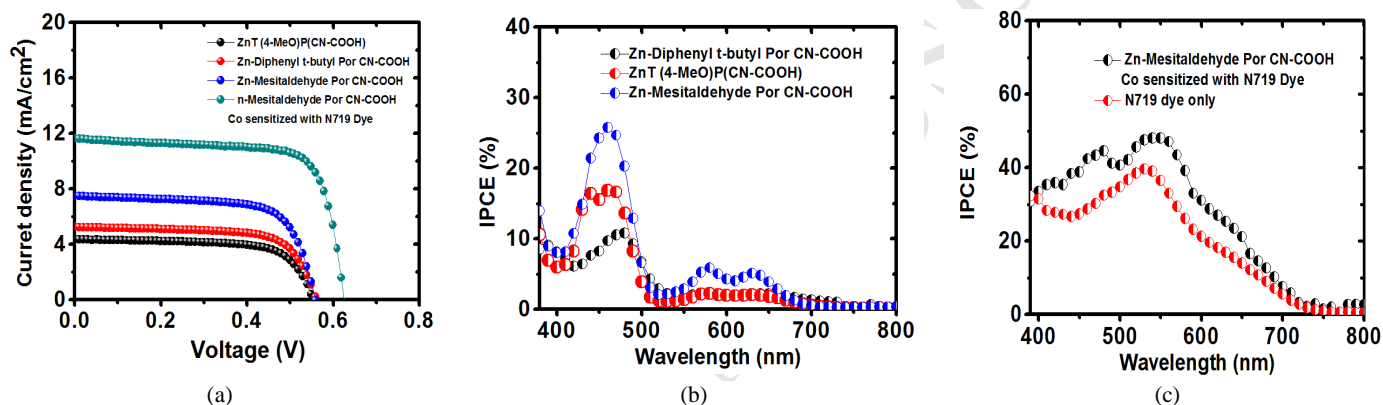


Fig. 4 (a) The typical I-V characteristics of the DSSCs using Zn(II) porphyrin dyes. IPCE action spectra of (b) Zn(II) porphyrin dyes and (c) ZnT(4-Mes)P(CN-COOH)(N719 dye) and N719 dye only

3.6 Electrochemical Impedance Spectroscopy

Electrochemical impedance spectroscopy (EIS) is a powerful tool to analyze interfacial and charge-transfer processes in the DSSC.⁶³ Figure 5 shows the Nyquist plots for solar cells based on synthesized Zn(II) porphyrin sensitizers under a bias voltage of -0.6 V in dark condition. Three semicircles are observed in Nyquist plots. The first semicircle is ascribed to the charge transfer resistance at the counter electrode-electrolyte interface in the high frequency region. The larger semicircle is associated with interfacial charge transfer resistances (R_{ct}) at the TiO₂-dye-electrolyte interface in the middle frequency region and low frequency region is assigned to impedance related to ion diffusion resistance in the electrolyte of the solar cell.

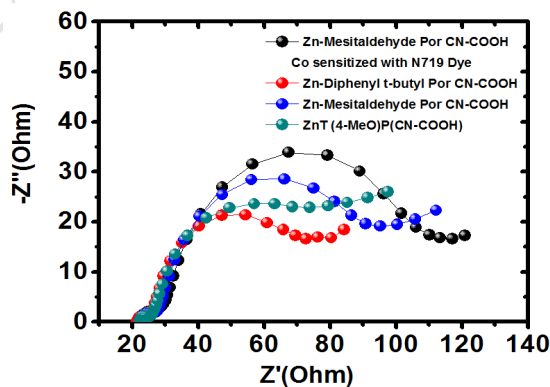


Fig. 5 Nyquist plots for synthesized Zn(II) porphyrin sensitizers under forward bias voltage of -0.6 V in dark condition.

Table 4. Electrochemical Impedance spectroscopy parameters of Zn(II) porphyrins under a bias voltage of -0.6 V in dark condition.

Zn-Porphyrin dyes	$R_{ct}(\Omega)$	$C_{\mu}(\mu\text{F}/\text{cm}^2)$	$\tau_r(\text{ms})$	IPCE
ZnT(Mes)P(CN-COOH)	94	8.3	7.8	27
ZnT(4-MeO)P(CN-COOH)	48	6	2.88	19
ZnT(4- <i>t</i> -Bu)P(Ph ₂)(CN-COOH)	65	4.4	2.73	13
ZnT(Mes)P(CN-COOH)(N719 dye)	108	10.2	12	50

R_{ct} defines the charge recombination rate between injected electrons and electron acceptors (I_3^-) in the electrolyte and a higher value R_{ct} slow down the electron transfer between the electrolyte and the TiO_2 with increase in the V_{oc} values.^{64,65} R_{ct} is related to the charge recombination rate between injected electrons and electron acceptors (I_3^-) in the electrolyte and a large R_{ct} implies slow electron transfer between the electrolyte and the TiO_2 , resulting in an increase in the V_{oc} values.⁶⁶ The fitted R_{ct} increased in the order of ZnT(4-MeO)P(CN-COOH) < ZnT(4-*t*-Bu)P(CN-COOH) < ZnT(Mes)P(CN-COOH) < ZnT(4-Mes)P(CN-COOH)-Co-sensitized N719.

This trend is consistent with the order of V_{oc} . From the R_{ct} value, electron life time (τ) was obtained by implying the following equation, $\tau = R_{ct} \times C_{chem}$ (C_{chem} = Chemical capacitance).⁶⁶ The electron lifetime (τ) reflects the response time constant for recombination and which is positively correlated with V_{oc} . ZnT(4-Mes)P(CN-COOH)(N719) exhibited highest chemical capacitance as shown in table 4 and this is correlated with the charge recombination rate. A longer electron lifetime indicates the effective reduction of the reverse reaction of the injected electron (slower recombination rate) with the triiodide in the electrolyte and therefore a higher photovoltage.⁶⁷ For these dye molecules, the calculated electron lifetime values increased in the order of ZnT(4-*t*-Bu)P(CN-COOH) (2.73 ms) < ZnT(4-MeO)P(CN-COOH) (2.88 ms) < ZnT(Mes)P(CN-COOH) (7.8 ms) < ZnT(Mes)P(CN-COOH)(N719) (12 ms). ZnT(Mes)P(CN-COOH)co-sensitized N719 dye exhibited the high recombination resistance (108 Ω), high capacitance (10.2×10^{-3} F/cm²) and impressive longest electron lifetime (12 ms) which confirms the effective suppression of the electron recombination of the injected electron with the I_3^- in the electrolyte and TiO_2 electrode. This results in higher J_{sc} (11.8 mA/cm²), V_{oc} (0.630 V), FF (72 %) and a highest PCE value of 5.35% for ZnT(Mes)P(CN-COOH)(N719)dye. On the basis of above studies, ZnT(Mes)P(CN-COOH) showed better photovoltaic performance over other Zn(II) porphyrin dyes but its co-sensitization with N719 dye improved the efficiency of the cells due to its relatively increased photocurrent voltage and effective retardation of dye aggregation. The EIS results of Zn(II) porphyrin dyes are in good agreement with the photovoltaic performance.

4. Conclusions

Three new β -functionalized push-pull Zn(II) porphyrin dyes have been successfully designed, synthesized by facile synthetic route in good yields and characterized by various spectroscopic techniques. These dyes exhibited remarkable red-shift as compared to ZnTPP due to the electron-withdrawing nature of cyanoacetic acid group and charge-transfer interactions. The decrement in the quantum yield and lifetime as well as the comparison of HOMO-LUMO energy levels of Zn(II) porphyrin dyes from cyclic voltammetry studies clearly suggest the feasibility of electron transfer for DSSC application. Photovoltaic studies of Zn(II) porphyrin dyes exhibited the power conversion efficiency from 1.72 to 3.13% but co-sensitization of Zn(II)T(Mes)P(CN-COOH) with N719 dye improved the PCE upto 5.35%. The overall power conversion efficiencies (PCE) and the IPCE values for the dyes follow the order as ZnT(4-*t*-Bu)P(CN-COOH) ($\eta = 1.72\%$) < ZnT(4-MeO)P(CN-COOH) ($\eta = 2.27\%$) < ZnT(Mes)P(CN-COOH) ($\eta = 3.13\%$) < ZnT(Mes)P(CN-COOH)(N719) ($\eta = 5.35\%$). This work demonstrates the effect of *meso*- and β -substituents on electronic spectral features and photovoltaic properties.

Acknowledgements

We are grateful for the support provided by Board of Research in Nuclear Science (2012/37C/61/BRNS/2776), Council of Scientific and Industrial Research (01(2694)/12/EMR-II) and Science and Engineering Research Board (SB/FT/CS-015/2012). KP and NS thank Ministry of Human Resource Development (MHRD), India for the senior research fellowship(SRF) and national postdoctoral fellowship (N-PDF), respectively.

^aDepartment of Chemistry, Indian Institute of Technology Roorkee, Roorkee - 247667, India. E-Mail: sankafcy@iitr.ac.in. Tel: +91-1332-284753; Fax: +91-1332-273560.

^bPolymers and Advanced Materials Laboratory, National Chemical Laboratory, Pune-411008, India. E-mail: k.krishnamoorthy@ncl.res.in; Tel: +91-20-2590-3075; Fax: +91-20-2590-2615.

Notes and References

1. Yao Z, Zhang M, Wu H, Yang L, Li R, Wang P. Donor/Acceptor Indenoperylene Dye for Highly Efficient Organic Dye-Sensitized Solar Cells. *J Am Chem Soc* 2015;137:3799–3802.
2. Kakiage K, Aoyama Y, Yano T, Oya K, Fujisawa JI, Hanaya M. Highly-efficient dye-sensitized solar cells with collaborative sensitization by silyl-anchor and carboxy-anchor dyes. *Chem Commun* 2015;51:15894–15897.
3. Mathew S, Yella A., Gao P, Humphry-Baker R, Curchod Basile FE, Ashari-Astani N, Tavernelli I, Rothlisberger U, Nazeeruddin KM, Grätzel M. Dye-sensitized solar cells with 13% efficiency achieved through the molecular engineering of porphyrin sensitizers. *Nat Chem* 2014;6:242–247.
4. Gao F, Wang Y, Zhang J, Shi D, Wang M, Baker RH, Wang P, Zakeeruddin SM, Grätzel M. A new heteroleptic ruthenium sensitizer enhances the absorptivity of mesoporous titania film for a high efficiency dye sensitized solar cell. *Chem Commun* 2008:2635–2637.
5. Yu QJ, Wang YH, Yi ZH, Zu NN, Zhang J, Zhang M, Wang P. High-Efficiency Dye-Sensitized Solar Cells: The Influence of Lithium Ions on Exciton Dissociation, Charge Recombination, and Surface States. *ACS Nano* 2010;4:6032–6038.
6. Mishra A, Fischer MKR, Bäuerle P. Metal-Free Organic Dyes for Dye-Sensitized Solar Cells: From Structure: Property Relationships to Design Rules. *Angew Chem Int Ed* 2009;48:2474–2499.
7. Chang S, Wang HD, Hua Y, Li Q, Xiao XD, Wong WK, Wong WY, Zhu XJ, Chen T. Conformational engineering of co-sensitizers to retard back charge transfer for high-efficiency dye-sensitized solar cells. *J Mater Chem A* 2013;1:11553–11558.
8. Hua Y, Chang S, Huang DD, Zhou X, Zhu XJ, Zhao ZJ, Chen T, Wong WY, Wong WK. Significant Improvement of Dye-Sensitized Solar Cell Performance Using Simple Phenothiazine-Based Dyes. *Chem Mater* 2013;25:2146–2153.
9. Cai X, Hou SC, Wu HW, Lv ZB, Fu YP, Wang D, Zhang C, Kafafy H, Chu ZZ, Zou DC. All carbon-electrode based fiber-shaped dye sensitized solar cells. *Phys Chem Chem Phys* 2012;14:125–130.
10. Shibano Y, Umeyama T, Matano Y, Imahori H. Electron-Donating Perylene Tetracarboxylic Acids for Dye-Sensitized Solar Cells. *Org Lett* 2007;9:1971–1974.
11. Ela SE, Yilmaz MD, Icli B, Dede Y, Icli S, Akkaya EU. A Panchromatic Boradiazaindacene (BODIPY) Sensitizer for Dye-Sensitized Solar Cells. *Org Lett* 2008;10:3299–3302.
12. Shin WS, Jeong HH, Kim MK, Jin SH, Kim MR, Lee JK, Lee JW, Gal YS. Effects of functional groups at perylene diimide derivatives on organic photovoltaic device application. *J Mater Chem* 2016;16:384–390.
13. Seo KD, Choi IT, Park YG, Kang S, Lee JY, Kim HK. Novel D-A- π -A Coumarin Dyes Containing Low Band-Gap Chromophores for Dye-Sensitized Solar Cells. *Dyes Pigm* 2012;94:469–474.
14. Wu W, Zhang J, Yang H, Jin B, Hu Y, Hua J, Jing C, Long Y, Tian H. Narrowing Band Gap of Platinum Acetylidyne Dye-Sensitized Solar Cell Sensitizers with Thiophene π -Bridges. *J Mater Chem* 2012;22:5382–5389.
15. Luo C, Bi W, Deng S, Zhang J, Chen S, Li B, Liu Q, Peng H, Chu J. Indolo[3,2,1-jk]carbazole Derivatives-Sensitized Solar Cells: Effect of π -Bridges on the Performance of Cells. *J Phys Chem C* 2014;118:14211–14217.
16. Yella A, Lee HW, Tsao HN, Yi C, Chandiran AK, Nazeeruddin MK. Porphyrin-sensitized solar cells with cobalt (II/III) based redox electrolyte exceed 12 percent efficiency. *Science* 2011;334:629–633.
17. Eu S, Katoh T, Umeyama T, Matano Y, Imahori H. Synthesis of sterically hindered phthalocyanines and their applications to dye-sensitized solar cells. *Dalton Trans* 2008: 5476–5483.
18. Bessho T, Zakeeruddin SM, Yeh C, Diau EW, Grätzel M. Highly efficient mesoscopic Dye-Sensitized Solar Cells based on donor-acceptor-substituted porphyrin. *Angew Chem Int Ed* 2010;49:6646–6649.
19. Imahori H, Matsubara Y, Iijima H, Umeyama T, Matano Y, Ito S. Effects of meso-diarylamino group of porphyrins as sensitizers in Dye-Sensitized Solar Cells on optical, electrochemical, and photovoltaic properties. *J Phys Chem C* 2010;114:10656–10665.
20. Yum J, Baranoff E, Kessler F, Moehl T, Ahmad S, Bessho T, Marchioro A, Ghadiri E, Moser J, Yi C, Nazeeruddin MK, Grätzel M. A Cobalt Complex Redox Shuttle for Dye-Sensitized Solar Cells with High Open-Circuit Potentials. *Nat Commun* 2012;3:631–638.
21. Deisenhofer J, Norris JR. *The Photosynthetic Reaction*. Academic Press, New York, 1993.
22. Itoh R, Fujita KI, Mu A, Kim DHT, Tai TT, Sagami I, Taketani S. Imaging of heme/hemeproteins in nucleus of the living cells expressing heme-binding nuclear receptors. *FEBS Lett* 2013;587:2131–2136.
23. Sudeep PK, Ipe BI, Thomas KG, George MV, Barazzouk S, Hotchandani S, Kamat PV. Fullerene-Functionalized Gold Nanoparticles. A Self-Assembled Photoactive Antenna-Metal Nanocore Assembly. *Nano Lett* 2002;2:29–35.
24. Kamat PV, Barazzouk S, Thomas KG, Hotchandani S. Electrodeposition of C₆₀ Cluster Aggregates on Nanostructured SnO₂ Films for Enhanced Photocurrent Generation. *J Phys Chem B* 2000;104:4014–4017.
25. Kumar R, Sankar M. Synthesis, Spectral, and Electrochemical Studies of Electronically Tunable β -Substituted Porphyrins with Mixed Substituent Pattern. *Inorg Chem* 2014;53:12706–12719.
26. Liu B, Zhu W, Wang Y, Wu W, Li X, Chen B, Long YT, Xie Y. Modulation of Energy Levels by Donor Groups: An Effective Approach for Optimizing the Efficiency of Zinc-Porphyrin Based Solar Cells. *J Mater Chem* 2012;22:7434–7444.
27. Prakash K, Kumar R, Sankar M. Mono- and tri-b-substituted unsymmetrical metalloporphyrins: synthesis, structural, spectral and electrochemical properties. *RSC adv* 2015;5:66824–66832.
28. Urbani M, Grätzel M, Nazeeruddin MK, Torres T. Meso-Substituted Porphyrins for Dye-Sensitized Solar Cells. *Chem Rev* 2014;114:12330–12396.
29. O'Regan B, Grätzel M. A low-cost, high-efficiency solar cell based on dye-sensitized colloidal TiO₂ films. *Nature* 1991;353:737–740.
30. Li LL, Diau EW. Porphyrin-sensitized solar cells. *Chem Soc Rev* 2013;42:291–304.
31. Wong WK, Zhu X, Wong WY. Synthesis, structure, reactivity and photoluminescence of lanthanide(III) monoporphyrinate complexes. *Coord Chem Rev* 2007;251:2386–2399.
32. Higashino T, Imahori H. Porphyrins as Excellent Dyes for Dye-Sensitized Solar Cells: Recent Developments and Insights. *Dalton Trans* 2015;44:448–463.

33. Imahori H, Umeyama T, Ito S. Large π -Aromatic Molecules as Potential Sensitizers for Highly Efficient Dye-Sensitized Solar Cells. *Acc Chem Res* 2009;42:1809-1818.
34. Wu SL, Lu HP, Yu HT, Chuang SH, Chiu CL, Lee CW, Diao EWG, Yeh CY. Design and characterization of porphyrin sensitizers with a push-pull framework for highly efficient dye-sensitized solar cells. *Energy Environ Sci* 2010;3:949-955.
35. Campbell WM, Burrell AK, Officer DL, Jolly KW. Porphyrins as light harvesters in the dye-sensitized TiO₂ solar cell. *Coord Chem Rev* 2004;248:1363-1379.
36. Lee CP, Lin RY, Lin LY, Li CT, Chu TC, Sun SS, Lin JT, Ho KC. Recent progress in organic sensitizers for dye-sensitized solar cells. *RSC Adv* 2015;5:23810-23825.
37. Ladomenou K, Kitsopoulos TN, Sharma GD, Coutsolelos AG. The importance of various anchoring groups attached on porphyrins as potential dyes for DSSC applications. *RSC Adv* 2014;4:21379-21404.
38. Yella A, Lee HW, Tsao HN, Yi C, Chandiran AK, Nazeeruddin MK, Diao EWG, Yeh CY, Zakeeruddin SM, Grätzel M. Porphyrin-Sensitized Solar Cells with Cobalt (II/III)-Based Redox Electrolyte Exceed 12% Efficiency. *Science* 2011;334:629-634.
39. Kang UH, Jeong MJ, Eom YK, Choi IT, Kwon SM, Yoo Y, Kim J, Kwon J, Park JH, Kim HK. Porphyrin Sensitizers with Donor Structural Engineering for Superior Performance Dye-Sensitized Solar Cells and Tandem Solar Cells for Water Splitting Applications. *Adv Energy Mater* 2017; 1602117
40. Wu CH, Pan TY, Hong SH, Wang CL, Kuo HH, Chu YY, Diao EWG, Lin CY. A fluorene-modified porphyrin for efficient dye-sensitized solar cells. *Chem Commun* 2012;48:4329-4331.
41. Wang CL, Chang YC, Lan CM, Lo CF, Diao EWG, Lin CY. Enhanced light harvesting with π -conjugated cyclic aromatic hydrocarbons for porphyrin-sensitized solar cells. *Energy Environ Sci* 2011;4:1788-1795.
42. Tanaka M, Hayashi S, Eu S, Umeyama T, Matano Y, Imahori H. Novel unsymmetrically π -elongated porphyrin for dye-sensitized TiO₂ cells. *Chem Commun* 2007;43:2069-2071.
43. Mai CL, Huang WK, Lu HP, Lee CW, Chiu CL, Liang YR, Diao EWG, Yeh CY. Synthesis and characterization of diporphyrin sensitizers for dye-sensitized solar cells. *Chem Commun* 2010;46:809-811.
44. Bessho T, Zakeeruddin SM, Yeh CY, Diao EWG, Grätzel M. Highly Efficient Mesoscopic Dye-Sensitized Solar Cells Based on Donor-Acceptor-Substituted Porphyrins. *Angew Chem Int Ed* 2010;122:6796-6799.
45. Chang S, Wang H, Hua Y, Li Q, Xiao X, Wong WK, Wong WY, Zhu X, Chen T. Conformational engineering of co-sensitizers to retard back charge transfer for high-efficiency dye-sensitized solar cells. *J Mater Chem A* 2013;1:11553-11558.
46. Wang Q, Campbell WM, Bonfantini EE, Jolley KW, Officer DL, Walsh PJ, Gordon K, Humphry-Baker R, Nazeeruddin MK, Grätzel M. Efficient Light Harvesting by Using Green Zn-Porphyrin-Sensitized Nanocrystalline TiO₂ Films. *J Phys Chem B* 2005;109:15397-15409.
47. Campbell WM, Jolley KW, Wagner P, Wagner K, Walsh PJ, Gordon KC, Schmidt-Mende L, Nazeeruddin MK, Wang Q, Grätzel M, Officer DL. Highly Efficient Porphyrin Sensitizers for Dye-Sensitized Solar Cells. *J Phys Chem C* 2007;111:11760-11762.
48. Ishida M, Park SW, Hwang D, Koo YB, Sessler JL, Kim DY, Kim D. Donor-Substituted β -Functionalized Porphyrin Dyes on Hierarchically Structured Mesoporous TiO₂ Spheres. Highly Efficient Dye-Sensitized Solar Cells. *J Phys Chem C* 2011;115:19343-19354.
49. Bhyrappa P, Sankar M, Varghese B. Mixed substituted porphyrins: Structural and electrochemical redox properties. *Inorg Chem* 2006;45:4136-4149.
50. Grover N, Sankar M, Song Y, Kadish KM. Asymmetrically Crowded "Push-Pull" Octaphenylporphyrins with Modulated Frontier Orbitals: Syntheses, Photophysical and Electrochemical Redox Properties. *Inorg Chem* 2016;55:584-597.
51. Bonfantini EE, Burrell AK, Campbell WM, Crossley MJ, Gosper JJ, Harding MM, Officer DL, Reid DCW. Efficient synthesis of free-base 2-formyl-5,10,15,20-tetraarylporphyrins, their reduction and conversion to [(porphyrin-2-yl)methyl]phosphonium salts. *J Porphyrins Phthalocyanines* 2002;6:708-719.
52. Bhyrappa P, Velkannan V, Maity A. Regioselective syntheses of 2,3-disubstituted-12-formyl-5,10,15,20-tetraphenylporphyrins and their metal complexes. *J Porphyrins Phthalocyanines* 2010;14:459-467.
53. Jaquinod L, Khoury RG, Shea KM. Regioselective syntheses and structural characterizations of 2,3-dibromo- and 2,3,7,8,12,13-hexabromo 5,10,15,20-tetraphenylporphyrins. *Tetrahedron* 1999;55:13151-13158.
54. Chahal MK, Sankar M. Porphyrin Chemodosimeters: Synthesis, Electrochemical Redox Properties and Selective 'Naked-eye' Detection of Cyanide Ions. *RSC Adv* 2015;5:99028-99036.
55. Reeta PS, Kandhadi J, Lingamallu G. One-pot synthesis of b-carboxy tetra aryl porphyrins: potential applications to dye-sensitized solar cells. *Tetrahedron Lett* 2010;51:2856-2867.
56. Kumar R, Yadav P, Rathi P, Sankar M. Photophysical, electrochemical redox, solvatochromism and anion sensing properties of β -tetra- and -octaphenylethynyl substituted meso-tetraphenylporphyrins. *RSC Adv* 2015;5:82237-82246.
57. Chahal MK, Sankar M, Butcher RJ. An Insight into Communication between β -olefin/phenyl olefin-mediated Acceptors and Porphyrin π -system: Way to establish Porphyrin based Chemodosimeters and Chemosensors. *Phys Chem Chem Phys* 2017;19:4530-4540.
58. Ishida M, Hwang D, Koo YB, Sung J, Kim DY, Sessler JL, Kim D. β -(Ethynylbenzoic acid)-substituted push-pull porphyrins: DSSC dyes prepared by a direct palladium-catalyzed alkynylation reaction. *Chem Commun* 2013;49:9164-9166.
59. Covezzi A, Orbelli Biroli A, Tessore F, Forni A, Marinotto D, Biagini P, Di Carlo G, Pizzotti M. 4D-p-1A type b-substituted ZnII-porphyrins: ideal green sensitizers for building-integrated photovoltaics. *Chem Commun* 2016;52:12642-12645.
60. Alder AD. A simplified synthesis for meso-tetraphenylporphyrin. *J Org Chem* 1967;34:476-479.
61. Zeng Z, Zhang B, Li C, Peng X, Liu X, Meng S, Feng Y. A key point of porphyrin structure affect DSSCs performance based on porphyrin sensitizers. *Dyes Pigments* 2014;100:278-285.
62. Lindsey J. Investigation of the Synthesis of Ortho-Substituted Tetraphenylporphyrins. *J Org Chem* 1989;58:828-836.
63. Barsoukov E, Macdonald JR. Impedance Spectroscopy: Theory, Experiment, and Applications; Eds.; John Wiley & Sons: Hoboken, NJ, 2005.
64. Han L, Koide N, Chiba Y, Mitate T. Modeling of an Equivalent Circuit for Dye-Sensitized Solar Cells. *Appl Phys Lett* 2004;84:2433-2435.
65. Wang Z, Wang H, Liang M, Tan Y, Cheng F, Sun Z, Xue S. Judicious Design of Indoline Chromophores for High Efficiency Iodine-Free Dye-Sensitized Solar Cells. *ACS Appl Mater Interfaces* 2014;6:5768-5778.

66. Kozma E, Concina I, Braga A, Borgese L, Depero LE, Vomiero A, Sberveglieri G, Catellani M. Metal-Free Organic Sensitizers With a Sterically Hindered Thiophene Unit for Efficient Dye-Sensitized Solar Cells. *J Mater Chem* 2011;21:13785-13788.
67. Wu Z, Li X, Agren H, Hua J, Tian H. Pyrimidine-2-carboxylic Acid as an Electron-Accepting and Anchoring Group for Dye-Sensitized Solar Cells. *ACS Appl Mater Interfaces* 2015;7:26355-26359.

ACCEPTED MANUSCRIPT

Electronic Supplementary Information

Facile Synthesis of β -Substituted “Push-Pull” Zn(II) Porphyrins for DSSC Applications

Kamal Prakash,^a Shweta Manchanda,^a Vediappan Sudhakar,^b Nidhi Sharma,^a Muniappan Sankar^{*a} and Kothandam Krishnamoorthy^{*b}

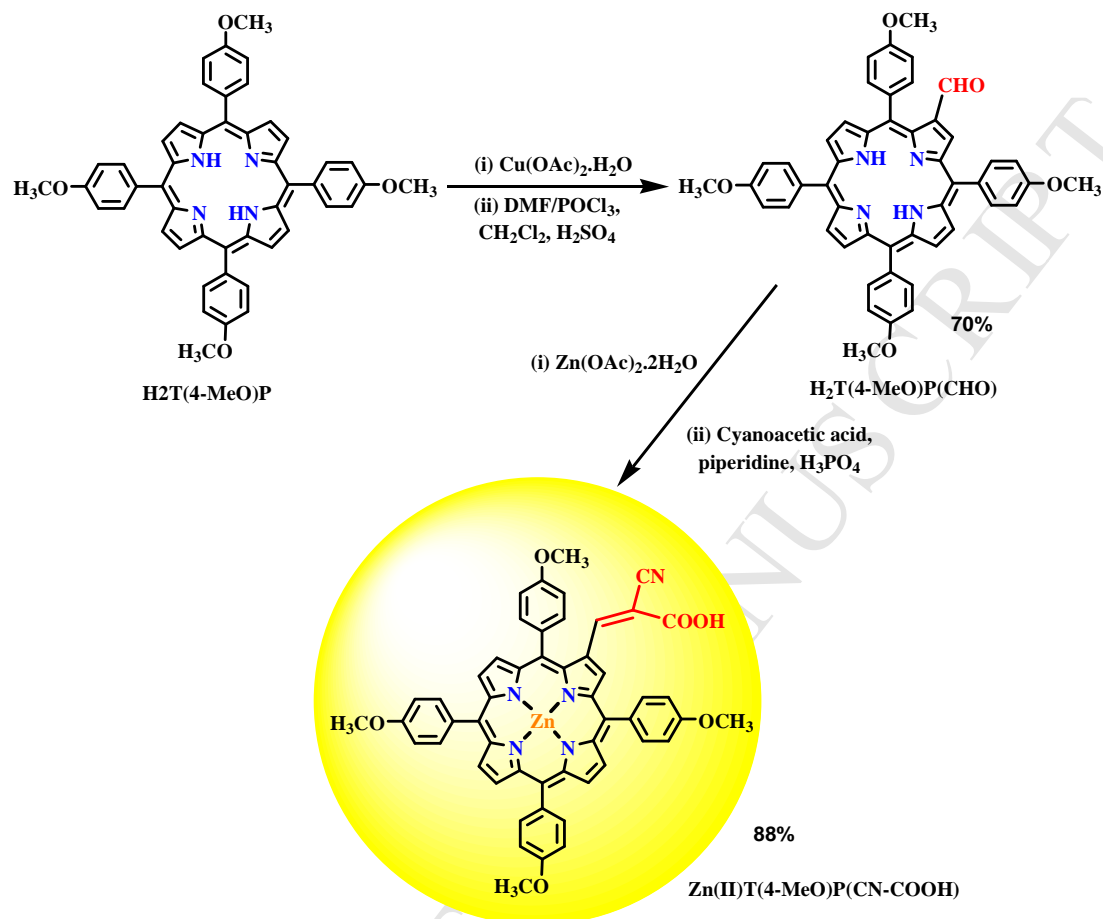
^aDepartment of Chemistry, Indian Institute of Technology Roorkee, Roorkee – 247667, India

^bPolymers and Advanced Materials Laboratory, National Chemical Laboratory, Pune-411008, India.

E-mail: k.krishnamoorthy@ncl.res.in; Tel: +91-20-2590-3075; Fax: +91-20-2590-2615.

Table of content	Page No.
Scheme S1. Synthetic Route of Zn(II)T(4-MeOPh)P(CN-COOH)	17
Fig. S1 UV-Vis Spectrum of (a) Free Base (4- <i>tbu</i>) Porphyrins (the intensity of Q band is enhanced by a factor of 5 for clarity.) (b) Zn(II) (4- <i>tbu</i>) Porphyrins in CHCl ₃ at 298K.	18
Fig. S2 UV-Vis Spectrum of (a) Free Base (4-MeO) Porphyrins (the intensity of Q band is enhanced by a factor of 5 for clarity.) (b) Zn(II) (4-MeO) Porphyrins in CHCl ₃ at 298 K.	18
Fig. S3 UV-Vis Spectrum of (a) Free Base (Mes) Porphyrins (the intensity of Q band is enhanced by a factor of 5 for clarity.) (b) Zn(II) (Mes) Porphyrins in CHCl ₃ at 298 K.	19
Fig. S4 UV-Vis Spectrum of Zn(II) mono-formylPorphyrins (the intensity of Q band is enhanced by a factor of 5 for clarity.) in CHCl ₃ at 298 K.	19
Fig. S5 Emission Spectrum of (a) Free Base tetraarylPorphyrins (b) mono-formylPorphyrins in CHCl ₃ at 298 K.	20
Fig. S6 Emission Spectrum of (a) Free Base (4- <i>tbu</i>) Porphyrins (b) Zn(II) Porphyrins in CHCl ₃ at 298 K.	20
Fig. S7 ¹ H-NMR spectrum of H ₂ T(4- <i>t</i> -Bu)P(CHO) in CDCl ₃ at 298 K	21
Fig. S8 ¹ H-NMR spectrum of H ₂ T(4- <i>t</i> -Bu)P(Br ₂)(CHO) in CDCl ₃ at 298 K	21
Fig. S9 ¹ H-NMR spectrum of H ₂ T(4- <i>t</i> -Bu)P(Ph ₂)(CHO) in CDCl ₃ at 298 K	22
Fig. S10 ¹ H-NMR spectrum of ZnT(4- <i>t</i> -Bu)P(Ph ₂)(CN-COOH) in DMSO at 298 K	22
Fig. S11 ¹ H-NMR spectrum of H ₂ T(4-MeO)P(CHO) in CDCl ₃ at 298 K	23
Fig. S12 ¹ H-NMR spectrum of ZnT(4-MeO)P(CHO) in CDCl ₃ at 298 K	23
Fig. S13 ¹ H-NMR spectrum of ZnT(4-MeO)P(CN-COOH) in DMSO- <i>d</i> ₆ at 298 K.	24
Fig. S14 ¹ H-NMR spectrum of H ₂ T(Mes)P(CHO) in CDCl ₃ at 298 K	24

Fig. S15 ^1H -NMR spectrum of $\text{ZnT}(\text{Mes})\text{P}(\text{CHO})$ in CDCl_3 at 298 K	25
Fig. S16 ^1H -NMR spectrum of $\text{ZnT}(\text{Mes})\text{P}(\text{CN-COOH})$ in $\text{DMSO-}d_6$ at 298 K	25
Fig. S17 ^{13}C -NMR spectrum of $\text{H}_2\text{T}(4-t\text{-Bu})\text{P}(\text{Br}_2)(\text{CHO})$ in CDCl_3 at 298 K	26
Fig. S18 ^{13}C -NMR spectrum of $\text{H}_2\text{T}(4-t\text{-Bu})\text{P}(\text{Ph}_2)(\text{CHO})$ in CDCl_3 at 298 K	26
Fig. S19 ^{13}C -NMR spectrum of $\text{H}_2\text{T}(4\text{-MeO})\text{P}(\text{CHO})$ in CDCl_3 at 298 K	27
Fig. S20 ^{13}C -NMR spectrum of $\text{ZnT}(4\text{-MeO})\text{P}(\text{CHO})$ in CDCl_3 at 298 K	27
Fig. S21 ^{13}C -NMR spectrum of $\text{ZnT}(4\text{-MeO})\text{P}(\text{CN-COOH})$ in $\text{DMSO-}d_6$ at 298 K	28
Fig. S22 ^{13}C -NMR spectrum of $\text{H}_2\text{T}(\text{Mes})\text{P}(\text{CHO})$ in CDCl_3 at 298 K	28
Fig. S23 ^{13}C -NMR spectrum of $\text{ZnT}(\text{Mes})\text{P}(\text{CHO})$ in CDCl_3 at 298 K	29
Fig. S24 ^{13}C -NMR spectrum of $\text{ZnT}(\text{Mes})\text{P}(\text{CN-COOH})$ in $\text{DMSO-}d_6$ at 298 K	29
Fig. S25 MALDI-TOF-MS of $\text{H}_2\text{T}(4\text{-}t\text{bu})\text{P}(\text{Br}_2)(\text{CHO})$	30
Fig. S26 MALDI-TOF-MS of $\text{H}_2\text{T}(4\text{-}t\text{-Bu})\text{P}(\text{Ph}_2)(\text{CHO})$	30
Fig. S27 MALDI-TOF-MS of $\text{ZnT}(4\text{-}t\text{bu})\text{P}(\text{Ph}_2)(\text{CN-COOH})$	31
Fig. S28 MALDI-TOF-MS of $\text{H}_2\text{T}(4\text{-MeO})\text{P}(\text{CHO})$	31
Fig. S29 MALDI-TOF-MS of $\text{ZnT}(4\text{-MeO})\text{P}(\text{CHO})$	32
Fig. S30 MALDI-TOF-MS of $\text{ZnT}(4\text{-MeO})\text{P}(\text{CN-COOH})$	32
Fig. S31 MALDI-TOF-MS of $\text{H}_2\text{T}(\text{Mes})\text{P}(\text{CHO})$	33
Fig. S32 MALDI-TOF-MS of $\text{ZnT}(\text{Mes})\text{P}(\text{CHO})$	33
Fig. S33 MALDI-TOF-MS of $\text{ZnT}(\text{Mes})\text{P}(\text{CN-COOH})$	34
Fig. S34 Cyclic Voltammograms of (a) free base tetraarylporphyrins (b) free base mono-formylporphyrins in CH_2Cl_2 at 298 K	34

**Scheme S1.** Synthetic Route of Zn(II)T(4-MeOPh)P(CN-COOH)

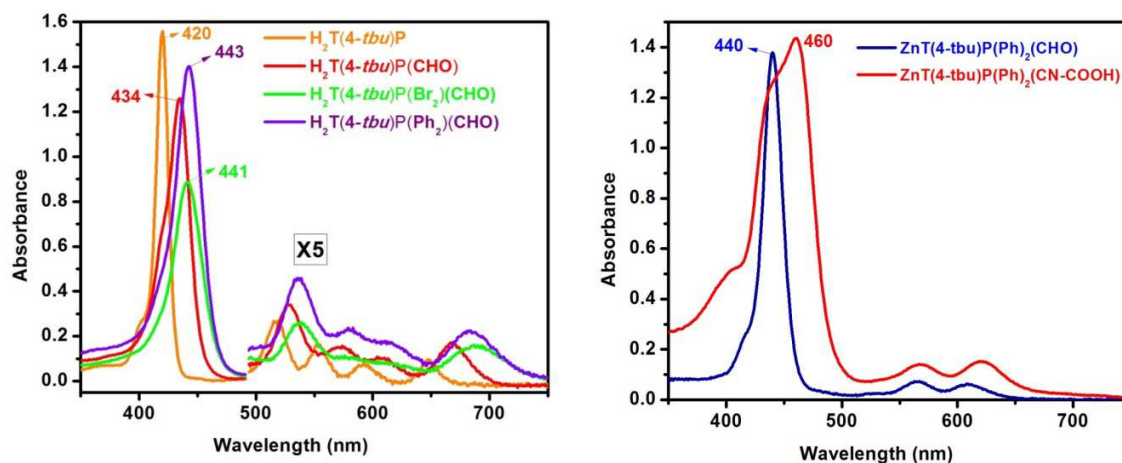


Fig. S1 UV-Vis Spectrum of (a) Free Base (4-*t*-Bu) Porphyrins (the intensity of Q band is enhanced by a factor of 5 for clarity.) (b) Zn(II) (4-*t*-bu) Porphyrins in CHCl_3 at 298 K.

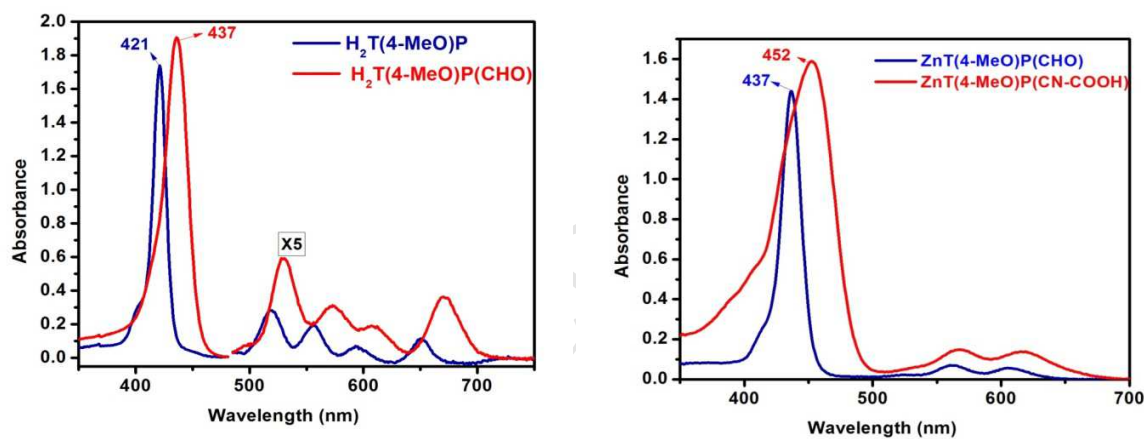


Fig. S2 UV-Vis Spectrum of (a) Free Base (4-MeO) Porphyrins (the intensity of Q band is enhanced by a factor of 5 for clarity.) (b) Zn(II) (4-MeO) Porphyrins in CHCl_3 at 298 K.

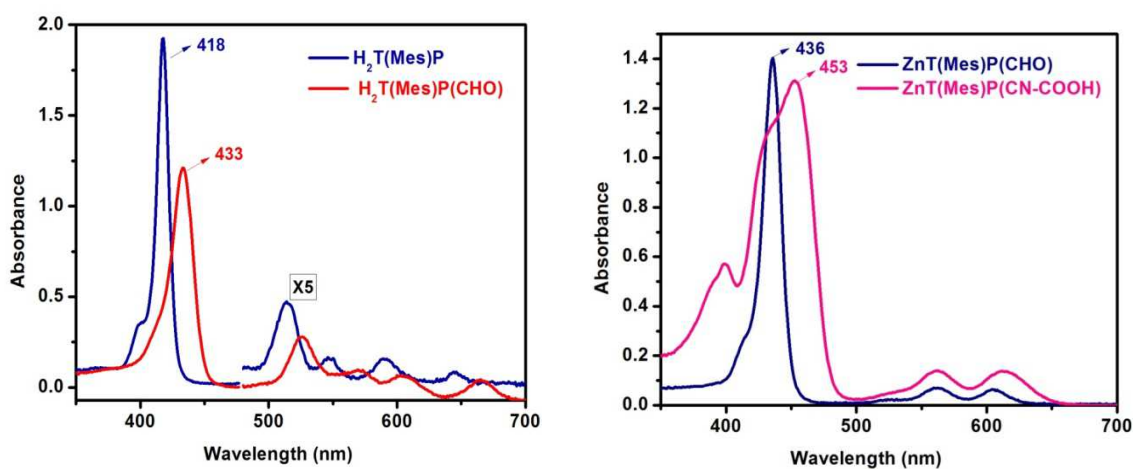


Fig. S3 UV-Vis Spectrum of (a) Free Base (Mes) Porphyrins (the intensity of Q band is enhanced by a factor of 5 for clarity.) (b) Zn(II) (Mes) Porphyrins in $CHCl_3$ at 298 K.

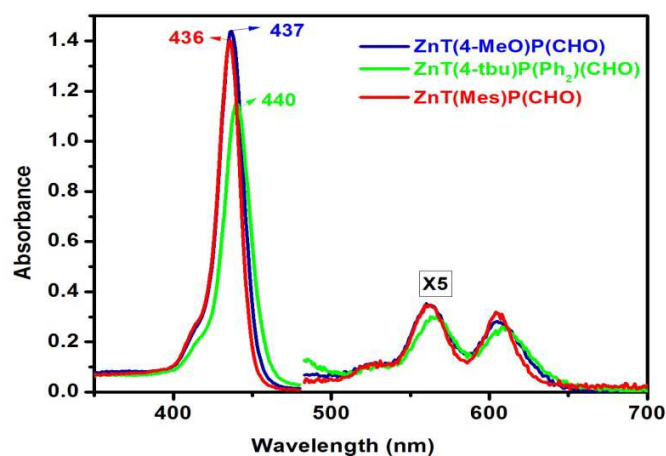


Fig. S4 UV-Vis Spectrum of Zn(II) mono-formyl Porphyrins (the intensity of Q band is enhanced by a factor of 5 for clarity.) in $CHCl_3$ at 298 K.

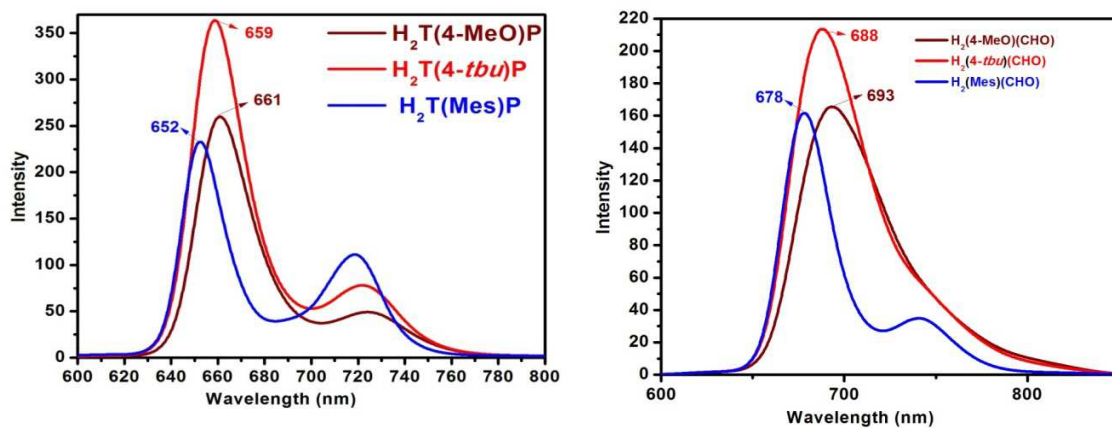


Fig. S5 Emission Spectrum of (a) Free Base tetraarylporphyrins (b) mono-formylporphyrins in CHCl_3 at 298 K.

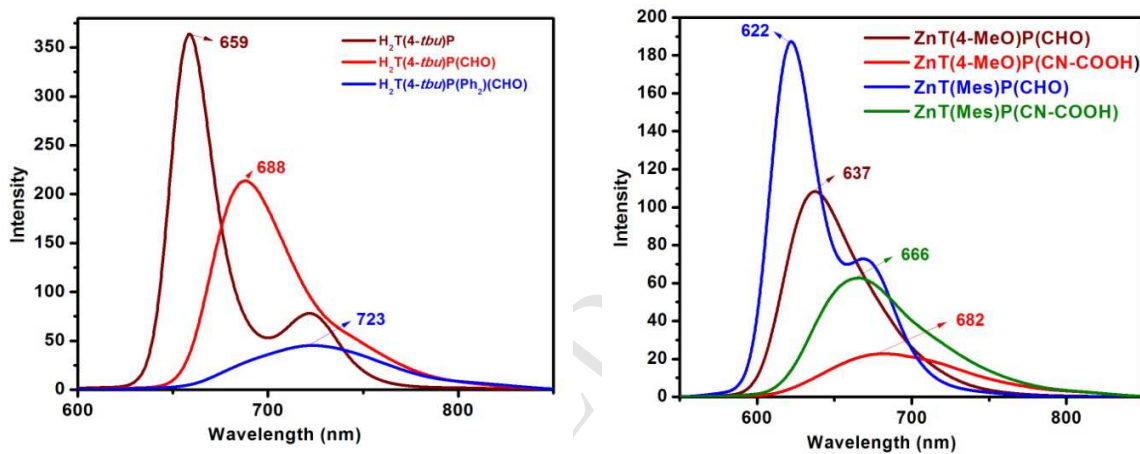


Fig. S6 Emission Spectrum of (a) Free Base (4-*t*-Bu)porphyrins (b) Zn(II) Porphyrins in CHCl_3 at 298 K.

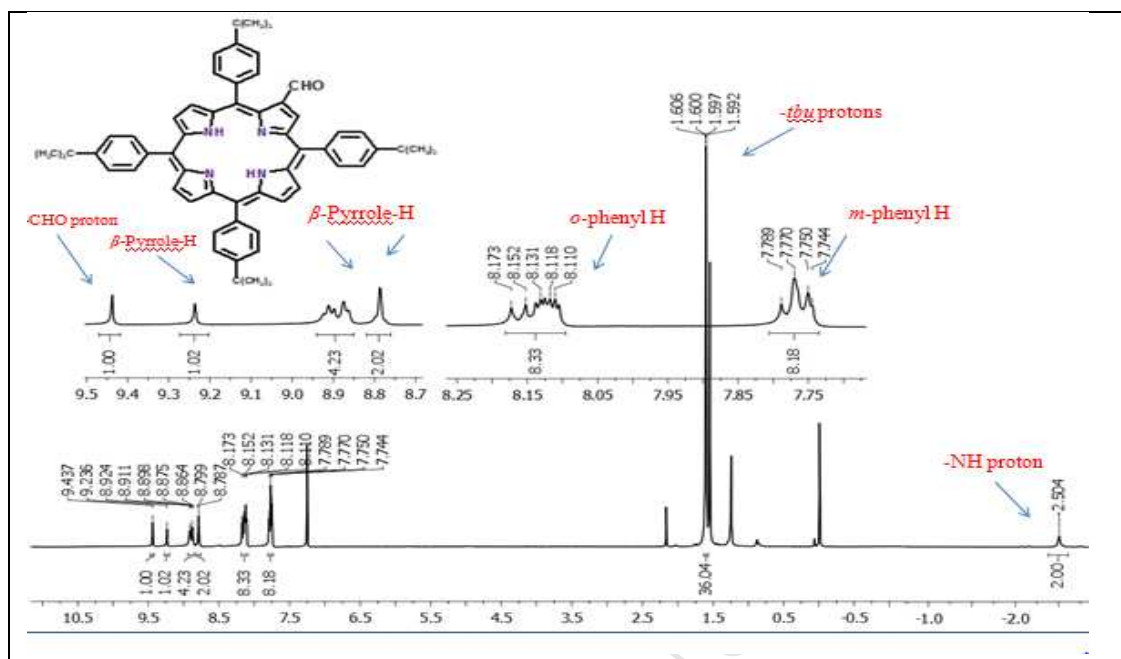


Fig. S7 ^1H -NMR spectrum of $\text{H}_2\text{T}(4-t\text{-Bu})\text{P}(\text{CHO})$ in CDCl_3 at 298 K

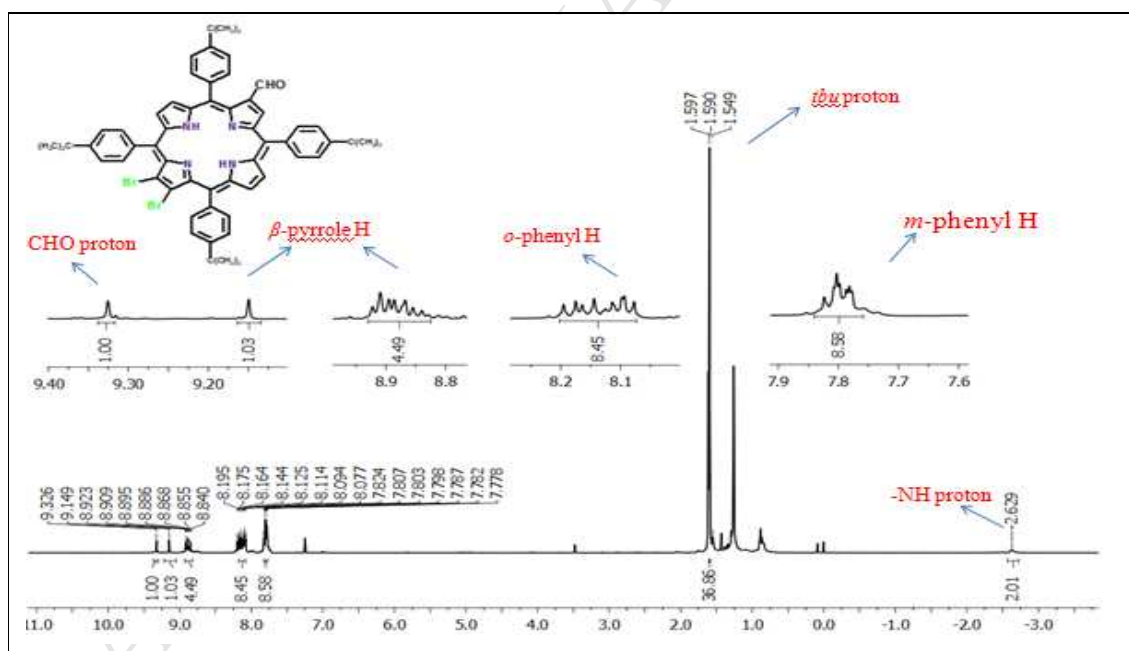


Fig. S8 ^1H -NMR spectrum of $\text{H}_2\text{T}(4-t\text{-Bu})\text{P}(\text{Br}_2)(\text{CHO})$ in CDCl_3 at 298 K

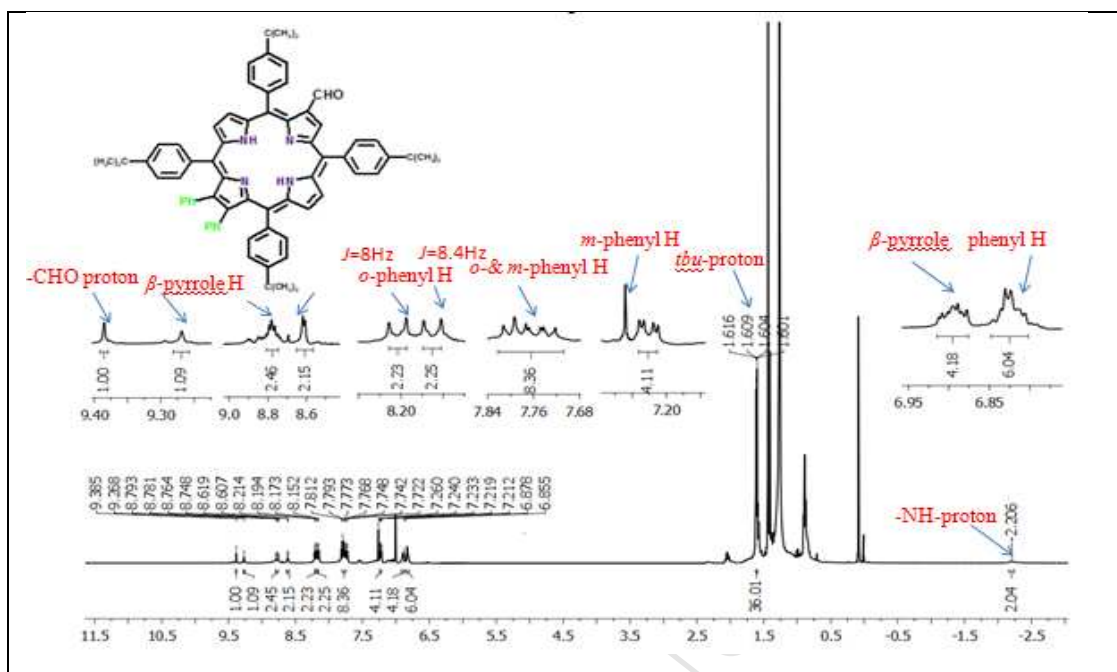


Fig. S9 $^1\text{H-NMR}$ spectrum of $\text{H}_2\text{T}(4\text{-}t\text{-Bu})\text{P}(\text{Ph}_2)(\text{CHO})$ in CDCl_3 at 298 K

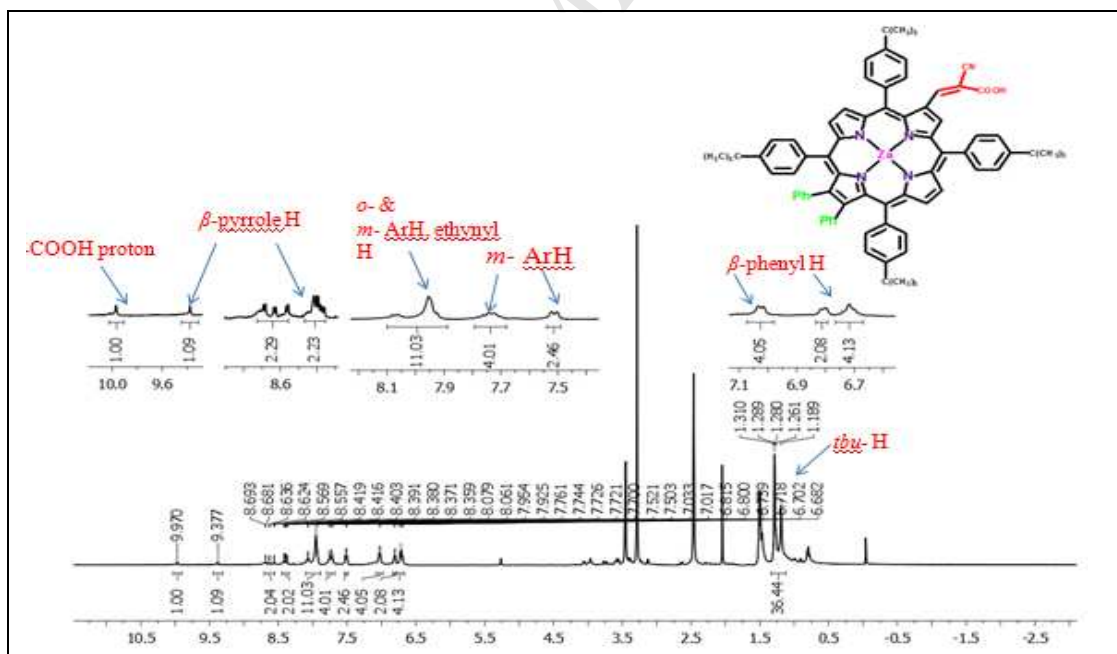


Fig. S10 $^1\text{H-NMR}$ spectrum of $\text{ZnT}(4\text{-}t\text{-Bu})\text{P}(\text{Ph}_2)(\text{CN-COOH})$ in $\text{DMSO-}d_6$ at 298 K

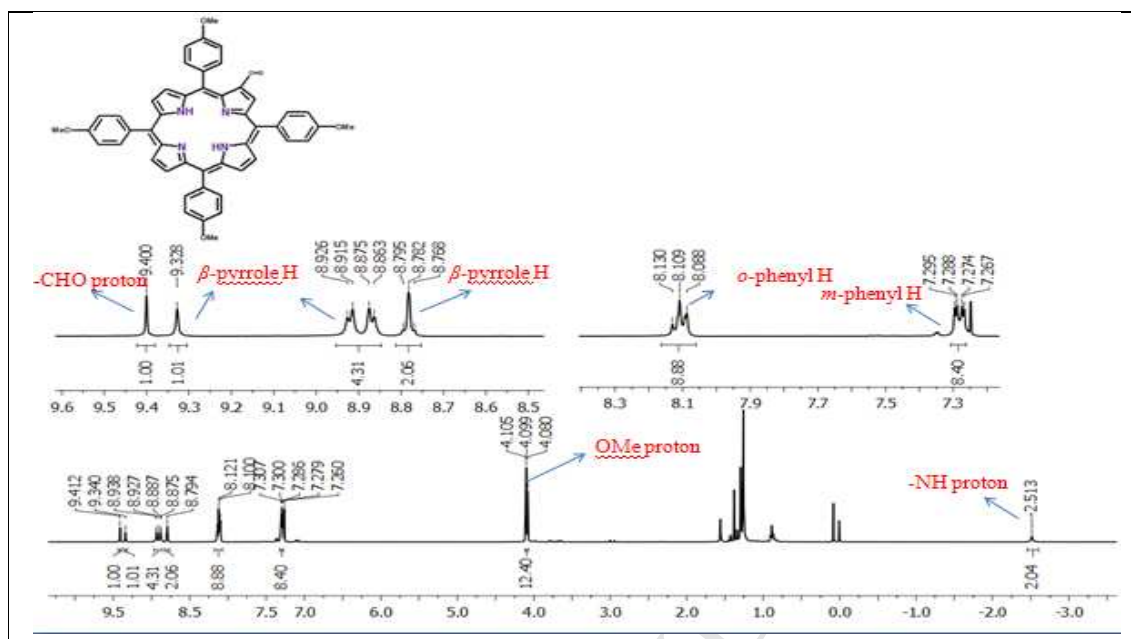


Fig. S11 ¹H-NMR spectrum of H₂T(4-MeO)P(CHO) in CDCl₃ at 298 K

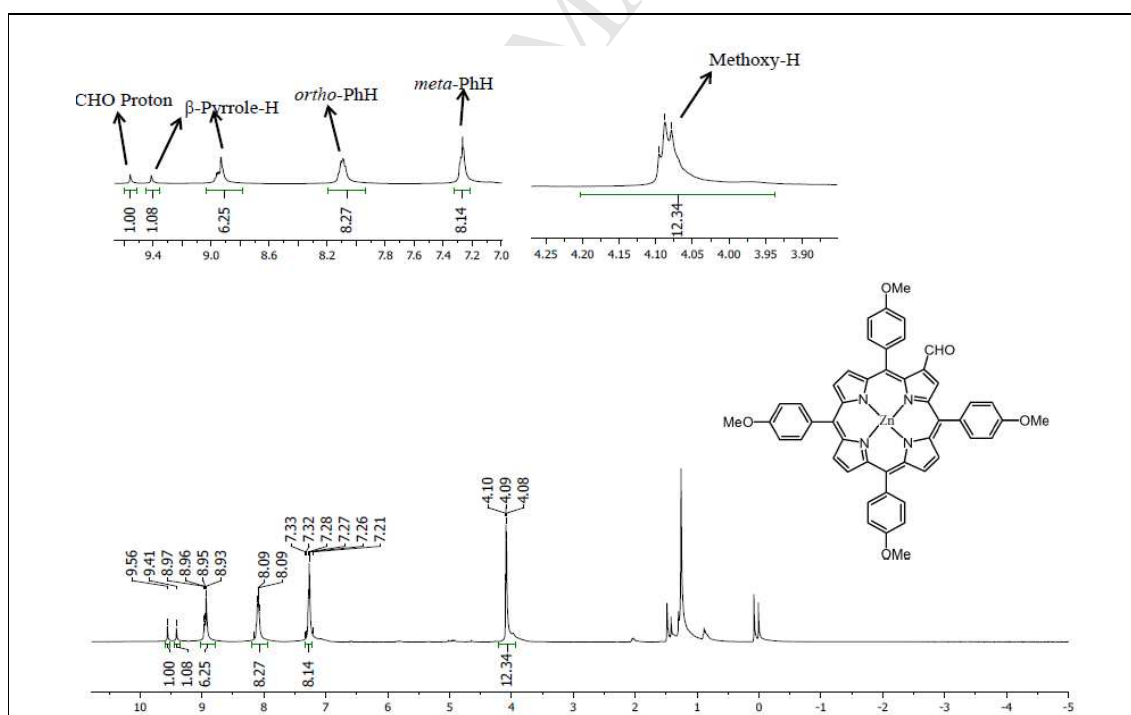


Fig. S12 ¹H-NMR spectrum of ZnT(4-MeO)P(CHO) in CDCl₃ at 298 K

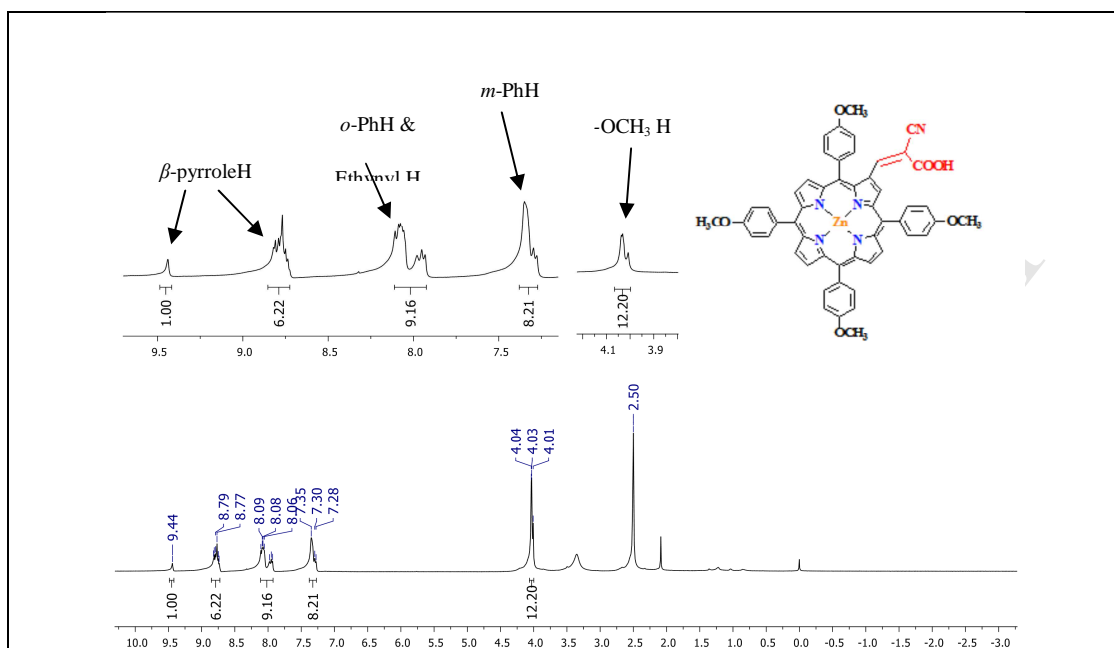


Fig. S13 ^{13}C -NMR spectrum of $\text{ZnT}(4\text{-MeO})\text{P}(\text{CN-COOH})$ in $\text{DMSO-}d_6$ at 298 K.

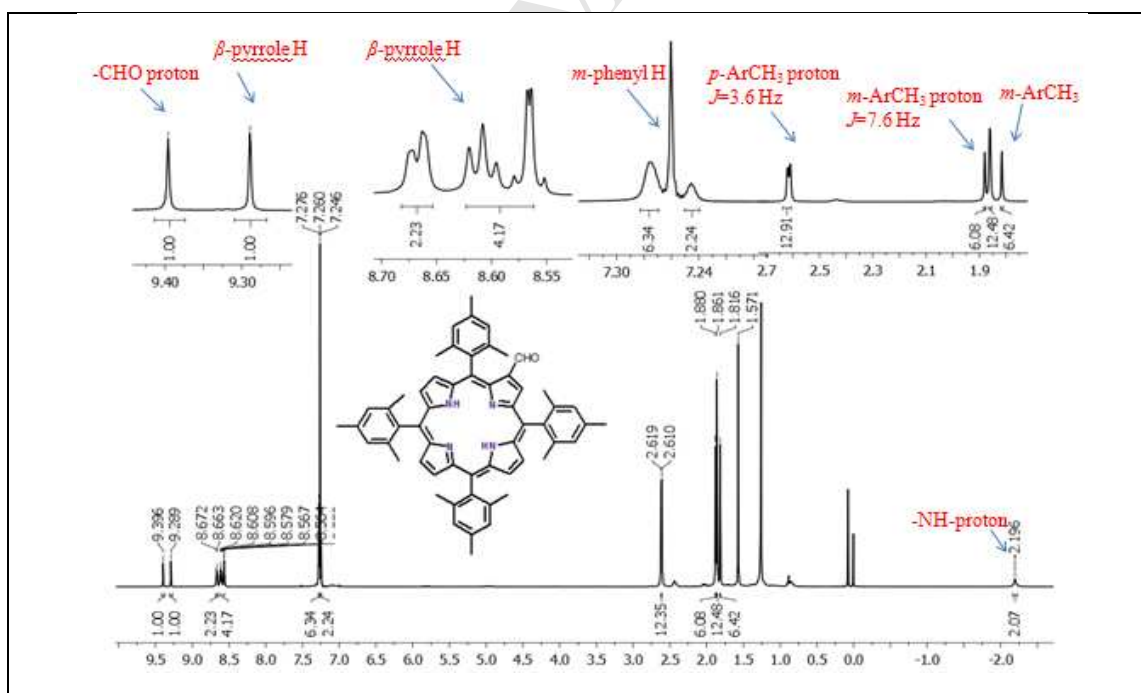


Fig. S14 ^1H -NMR spectrum of $\text{H}_2\text{T}(\text{Mes})\text{P}(\text{CHO})$ in CDCl_3 at 298 K

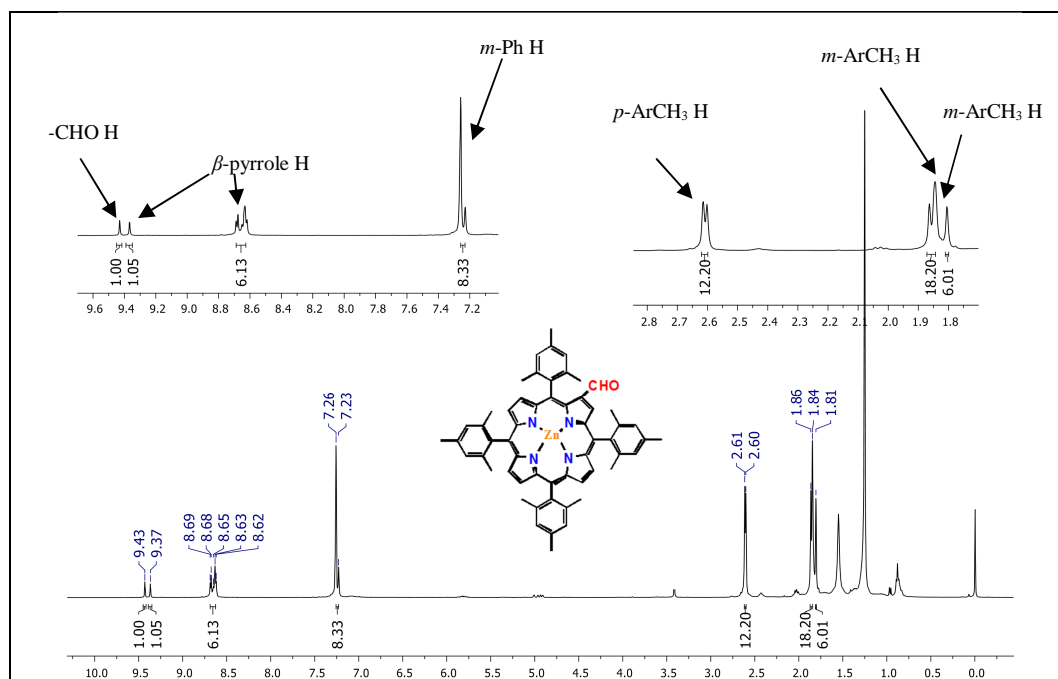


Fig. S15 $^1\text{H-NMR}$ spectrum of $\text{ZnT}(\text{Mes})\text{P}(\text{CHO})$ in CDCl_3 at 298 K

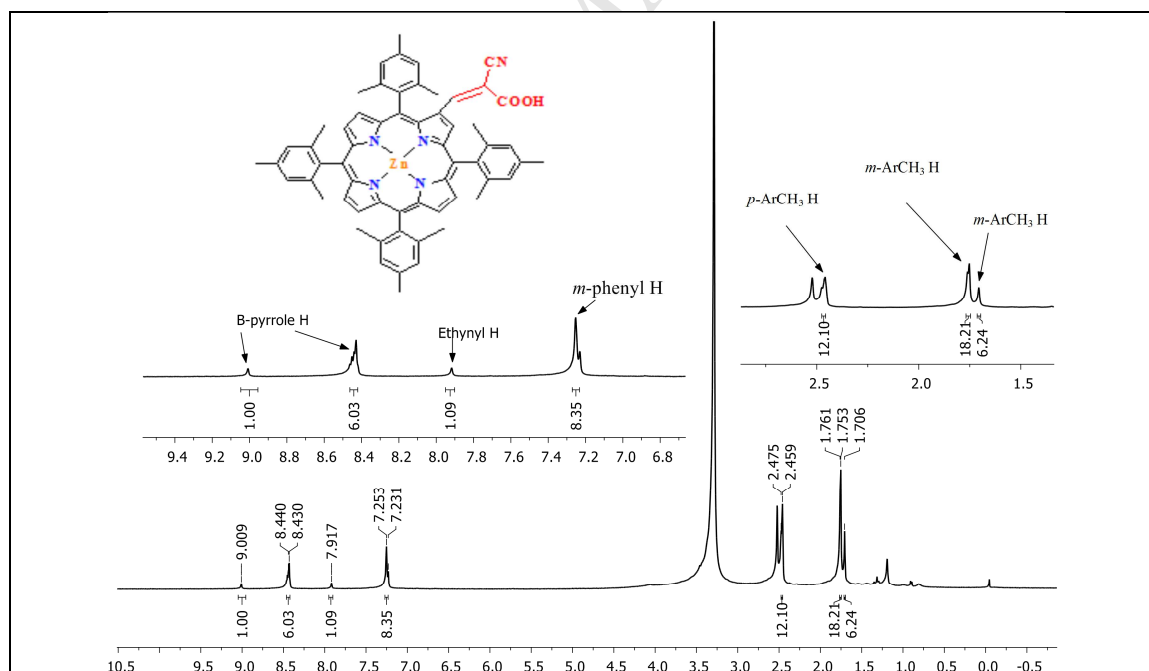


Fig. S16 $^1\text{H-NMR}$ spectrum of $\text{ZnT}(\text{Mes})\text{P}(\text{CN-COOH})$ in $\text{DMSO-}d_6$ at 298 K

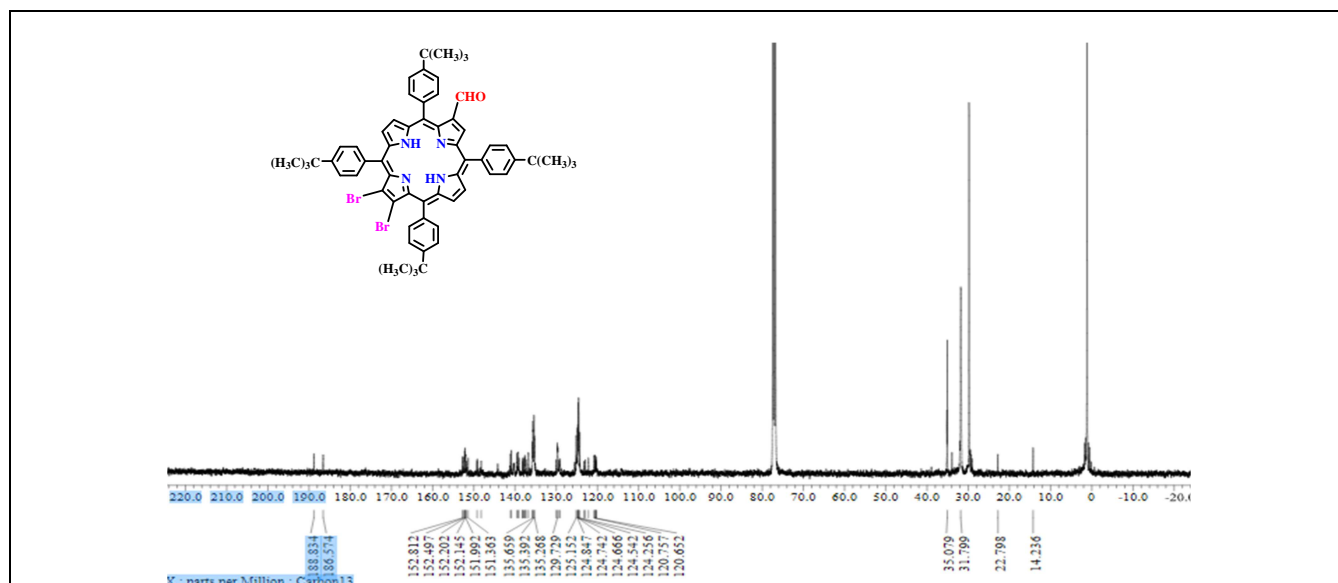


Fig. S17 ^{13}C -NMR spectrum of $H_2T(4-t-Bu)P(Br_2)(CHO)$ in $CDCl_3$ at 298 K

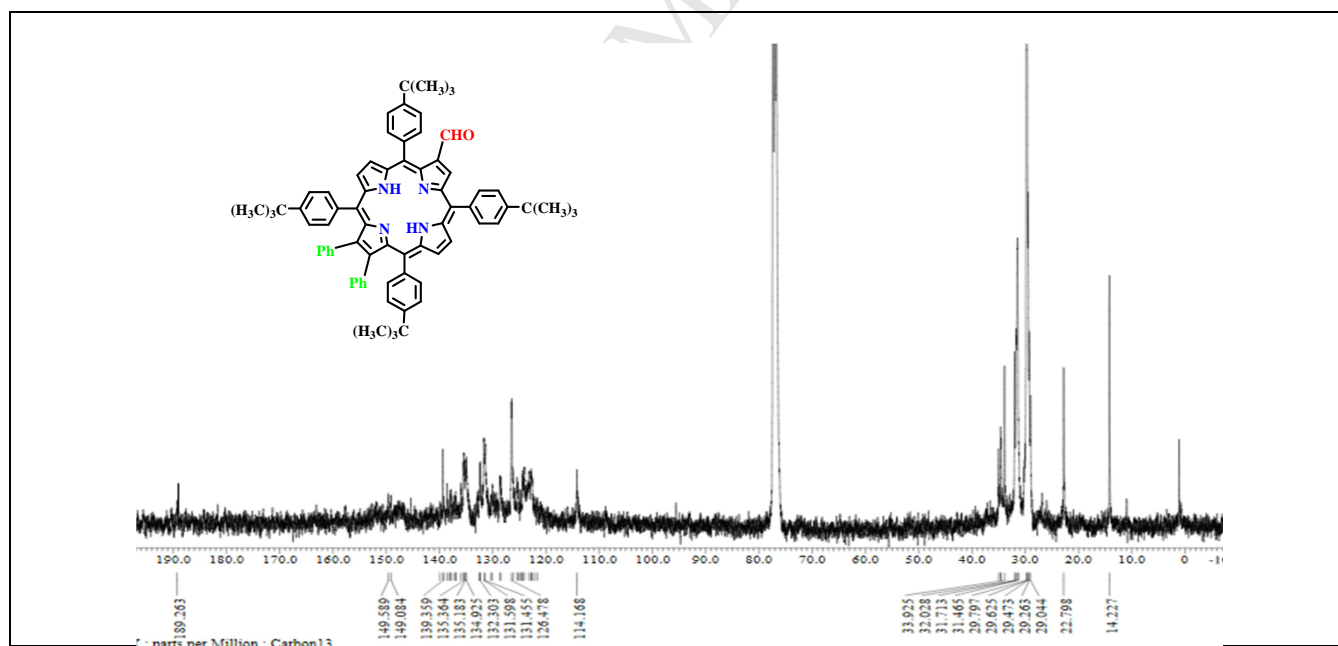


Fig. S18 ^{13}C -NMR spectrum of $H_2T(4-t-Bu)P(Ph_2)(CHO)$ in $CDCl_3$ at 298 K

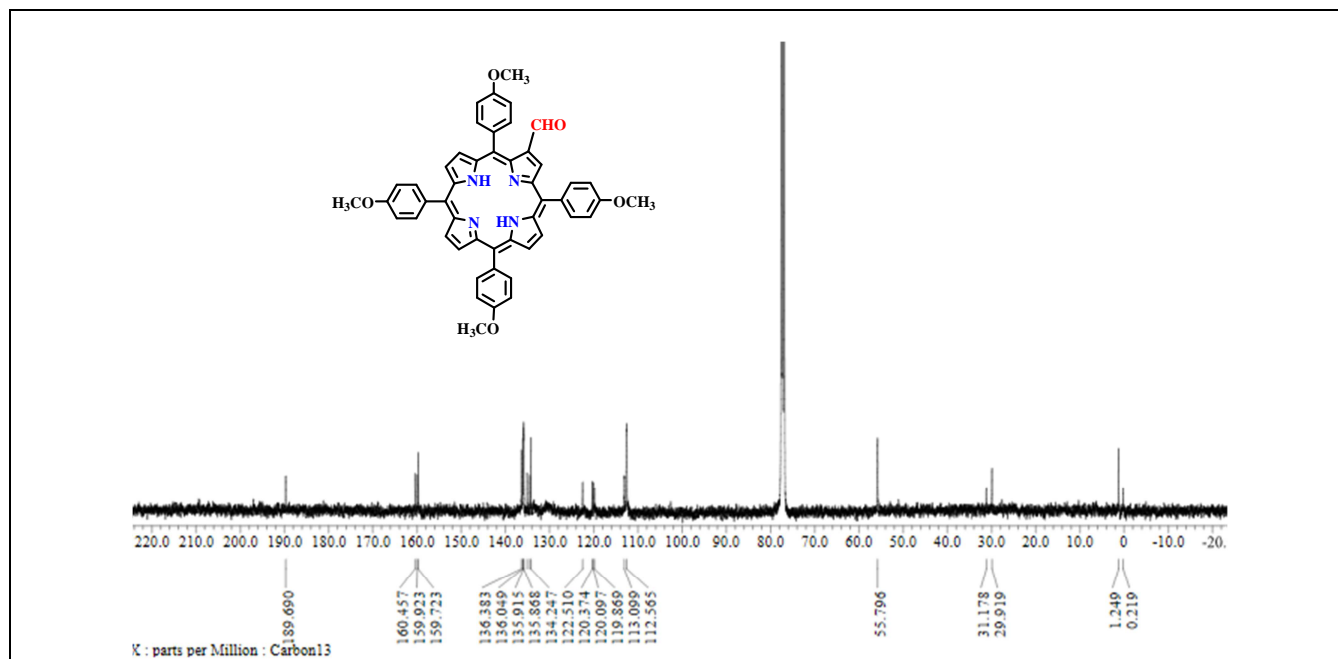


Fig. S19 ^{13}C -NMR spectrum of $H_2T(4-MeO)P(CHO)$ in $CDCl_3$ at 298 K

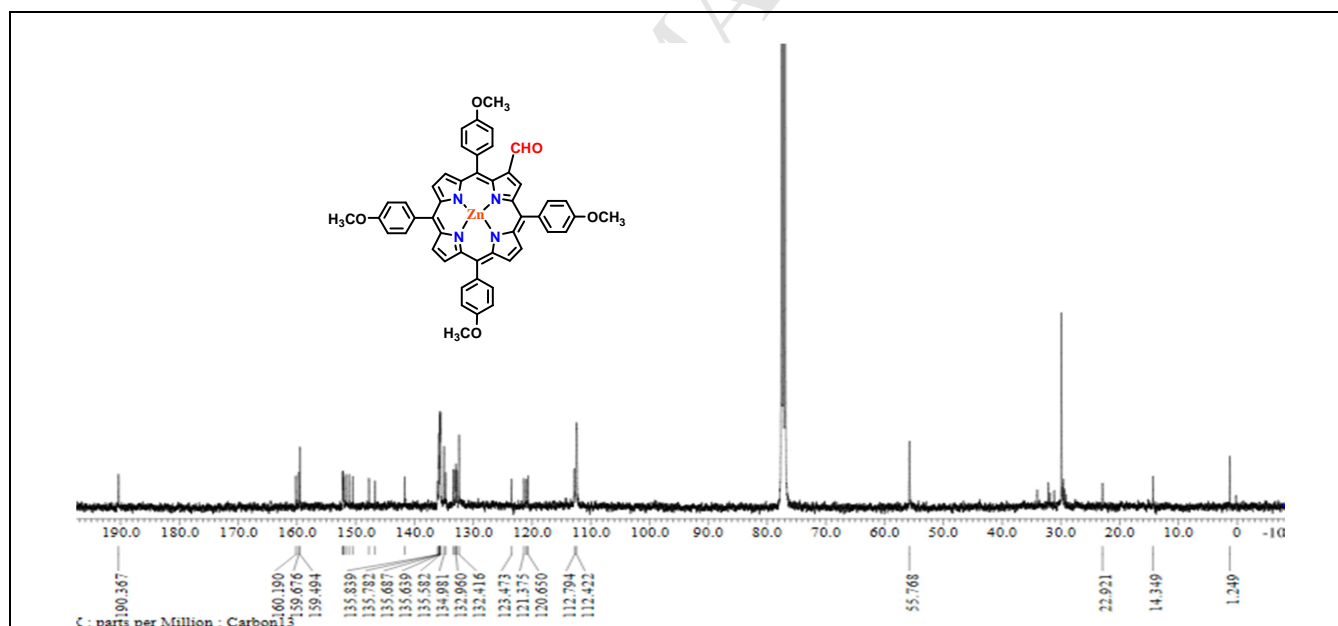


Fig. S20 ^{13}C -NMR spectrum of $ZnT(4-MeO)P(CHO)$ in $CDCl_3$ at 298 K

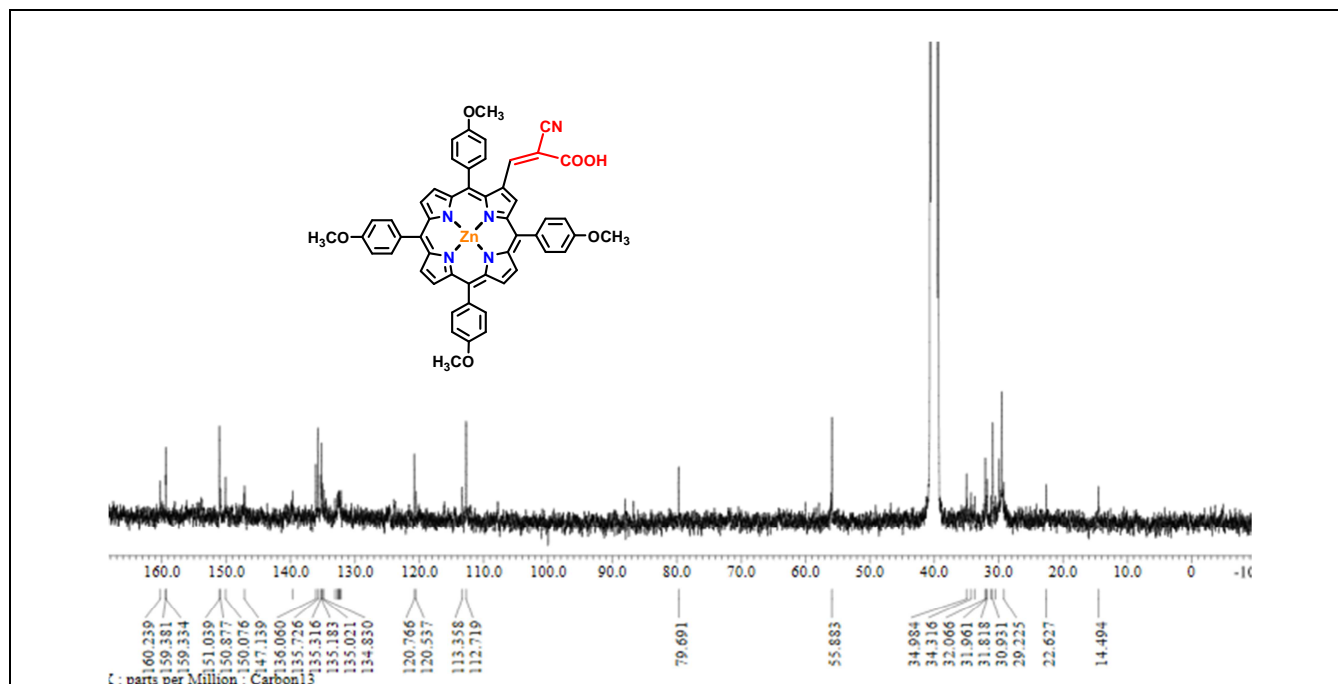


Fig. S21 ^{13}C -NMR spectrum of ZnT(4-MeO)P(CN-COOH) in $\text{DMSO-}d_6$ at 298 K

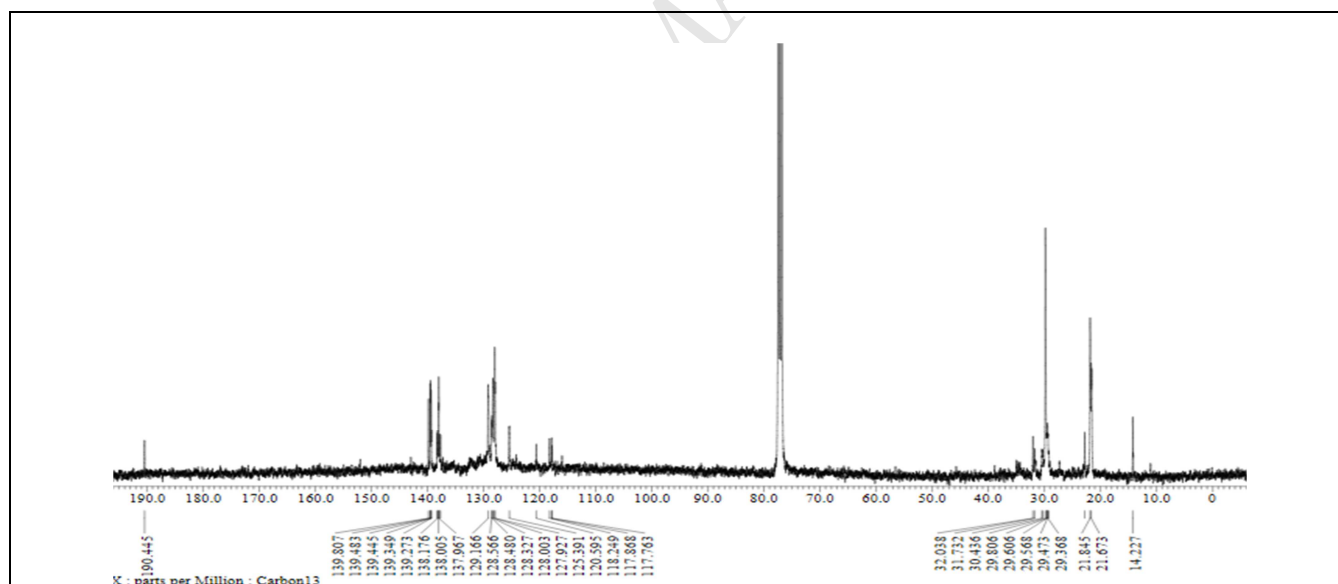


Fig. S22 ^{13}C -NMR spectrum of $\text{H}_2\text{T}(\text{Mes})\text{P}(\text{CHO})$ in CDCl_3 at 298 K

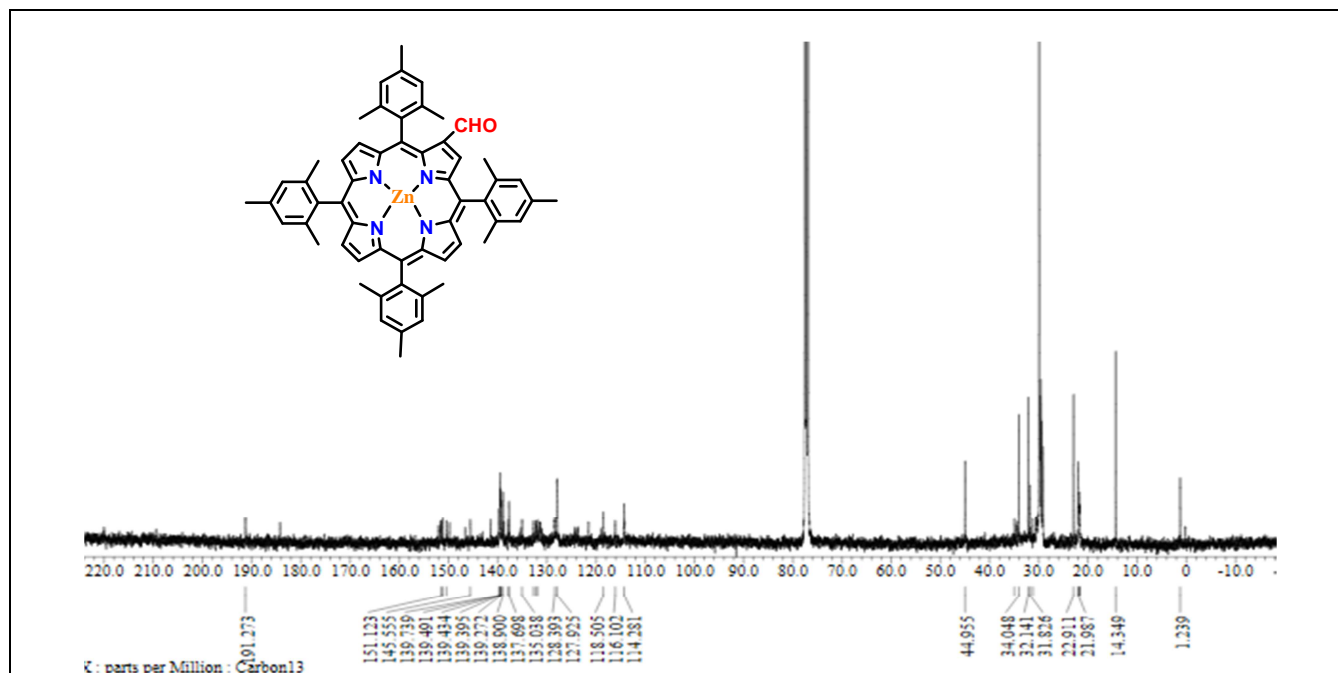


Fig. S23 ^{13}C -NMR spectrum of ZnT(Mes)P(CHO) in CDCl_3 at 298 K

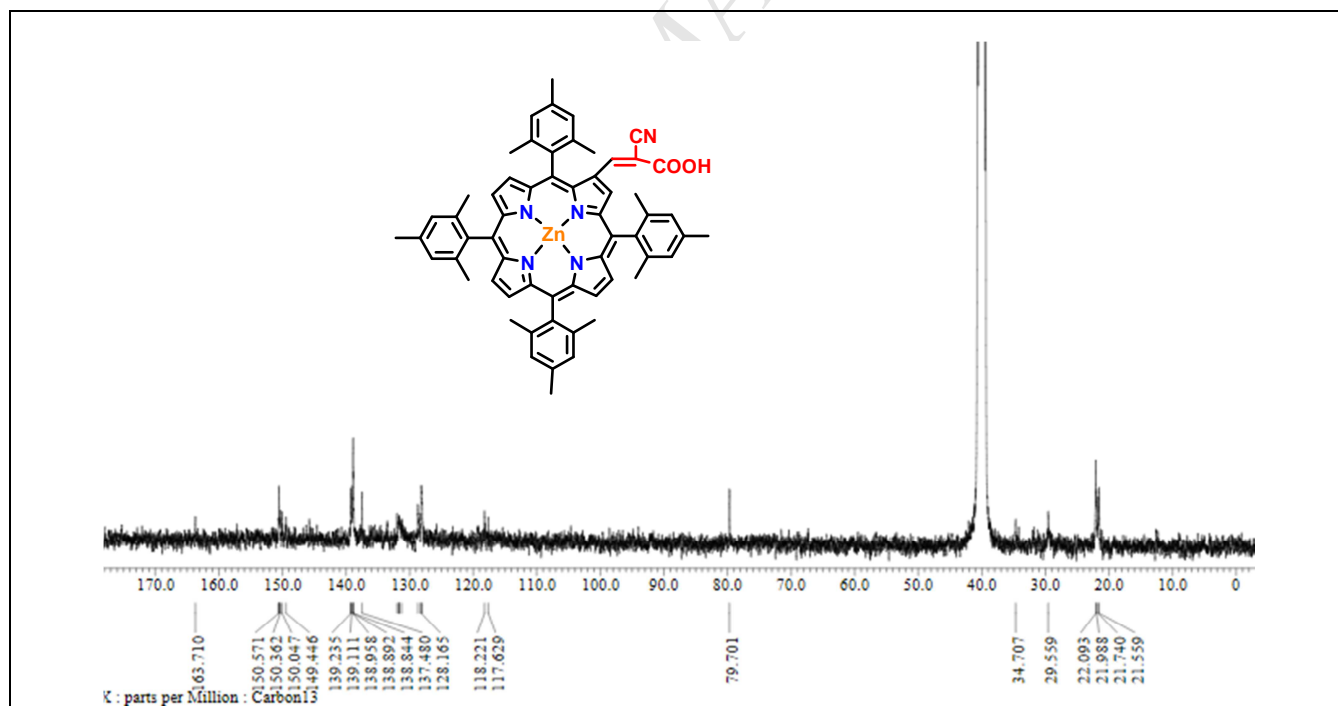


Fig. S24 ^{13}C -NMR spectrum of ZnT(Mes)P(CN-COOH) in $\text{DMSO-}d_6$ at 298 K

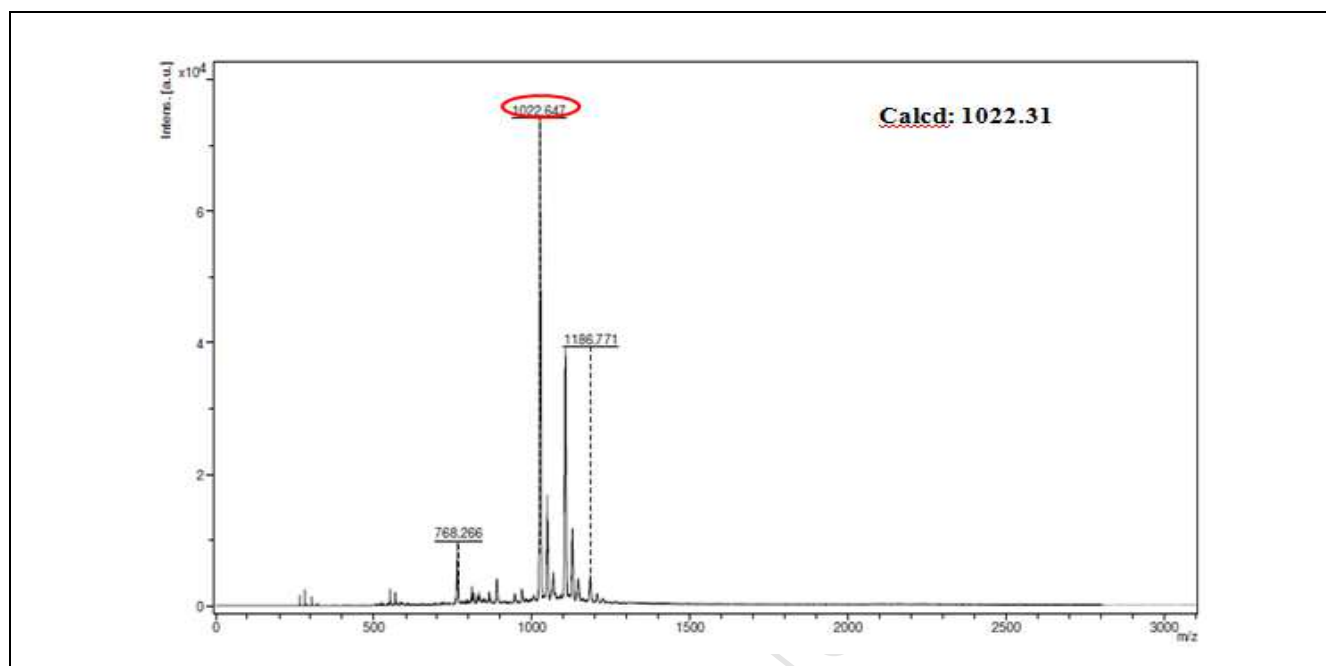


Fig. S25 MALDI-TOF-MS of H₂T(4-*t*-Bu)P(Br₂)(CHO)

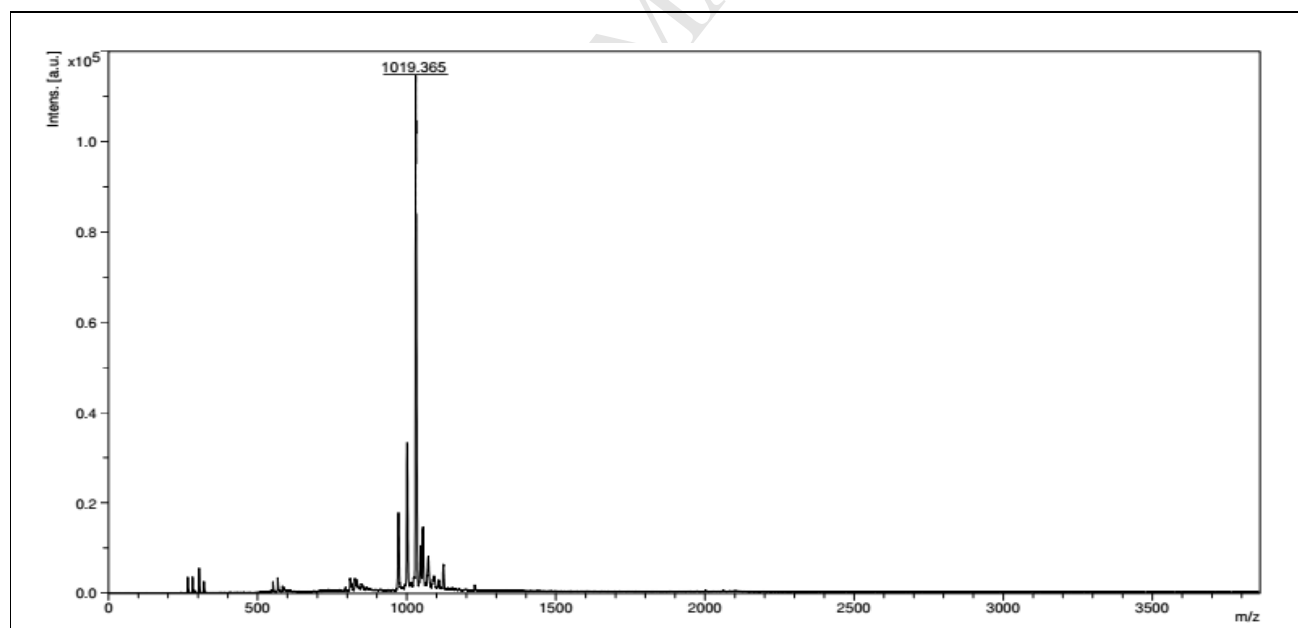


Fig. S26 MALDI-TOF-MS of H₂T(4-*t*-Bu)P(Ph₂)(CHO)

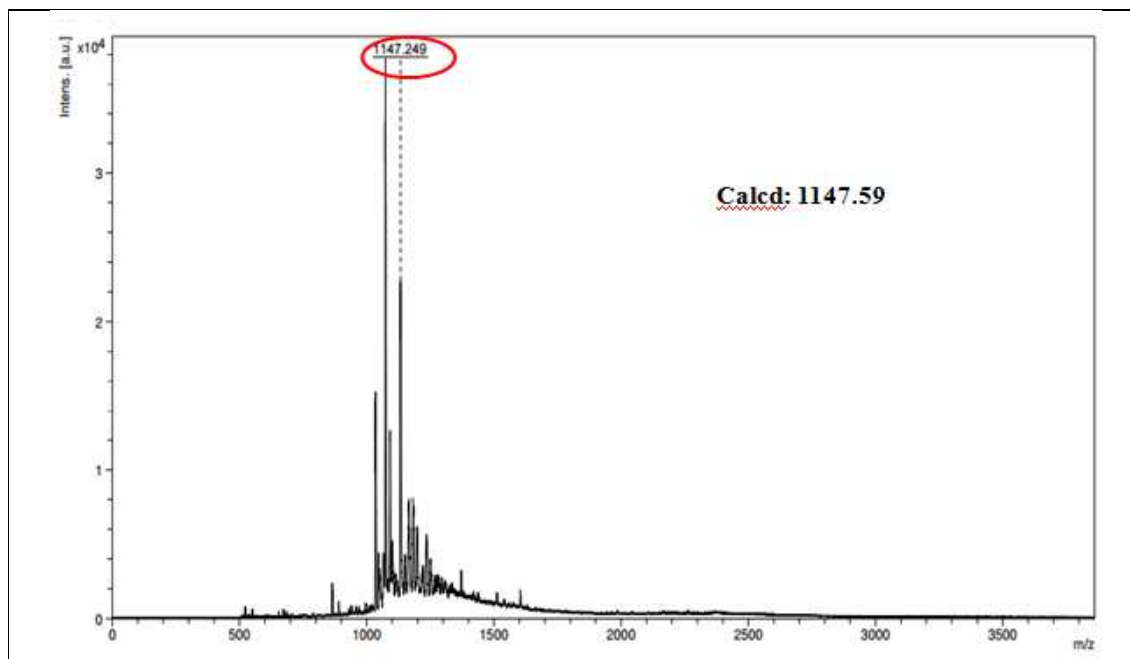


Fig. S27 MALDI-TOF-MS of $H_2T(4-t-Bu)P(Ph_2)(CN-COOH)$

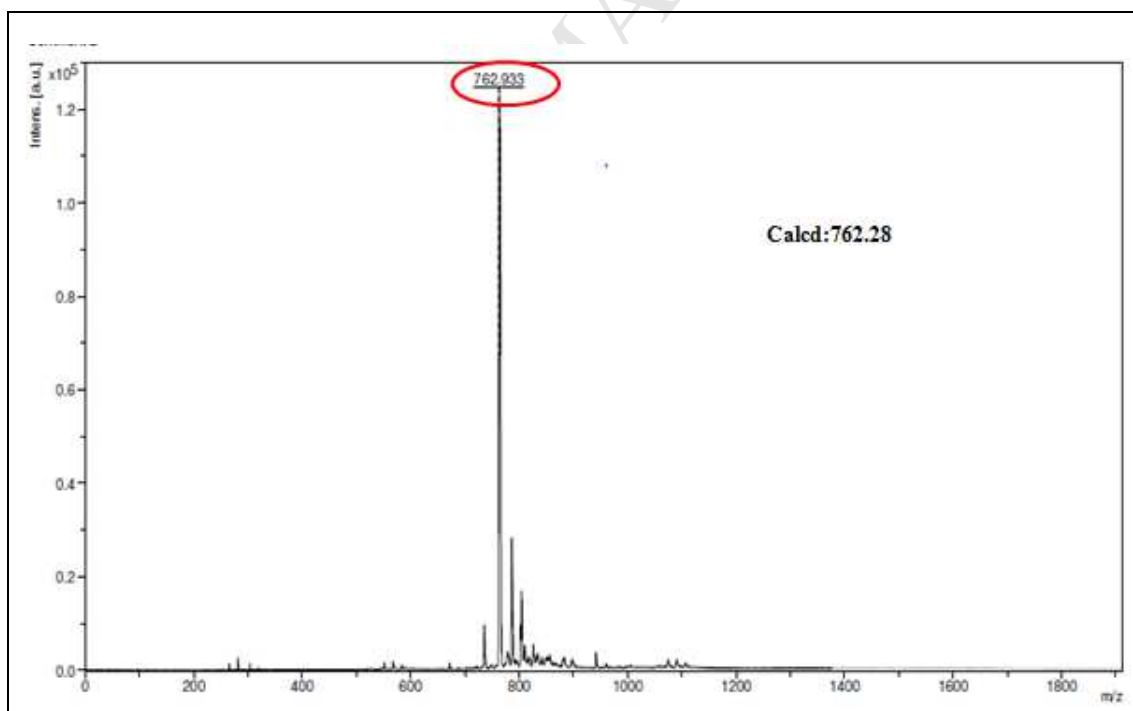


Fig. S28 MALDI-TOF-MS of $H_2T(4-MeO)P(CHO)$

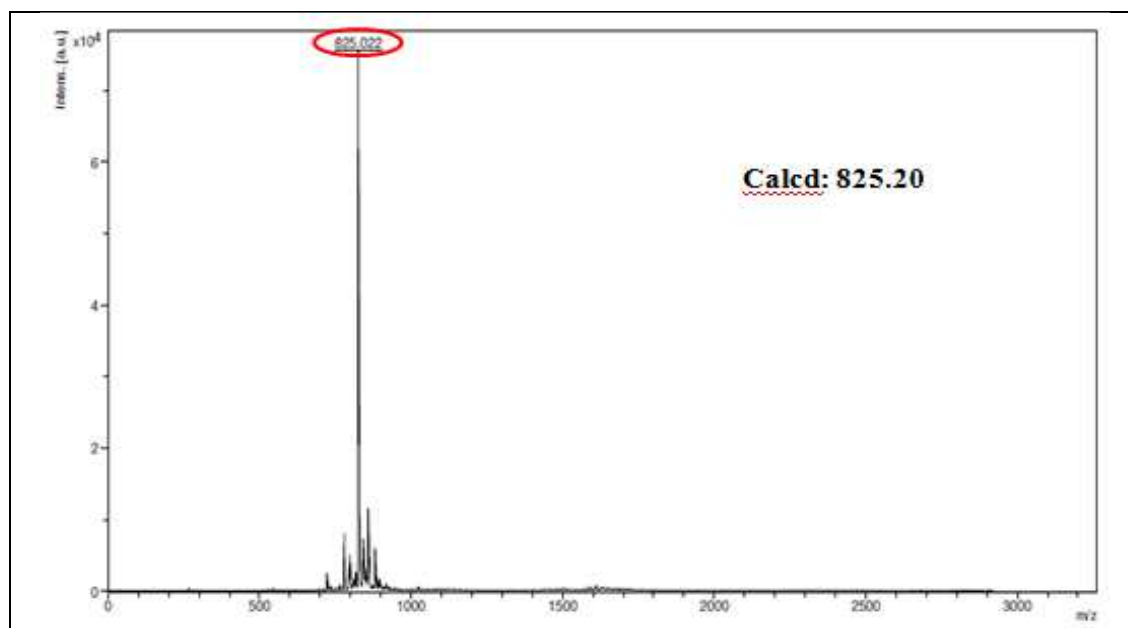


Fig S29 MALDI-TOF-MS of ZnT(4-MeO)PCHO

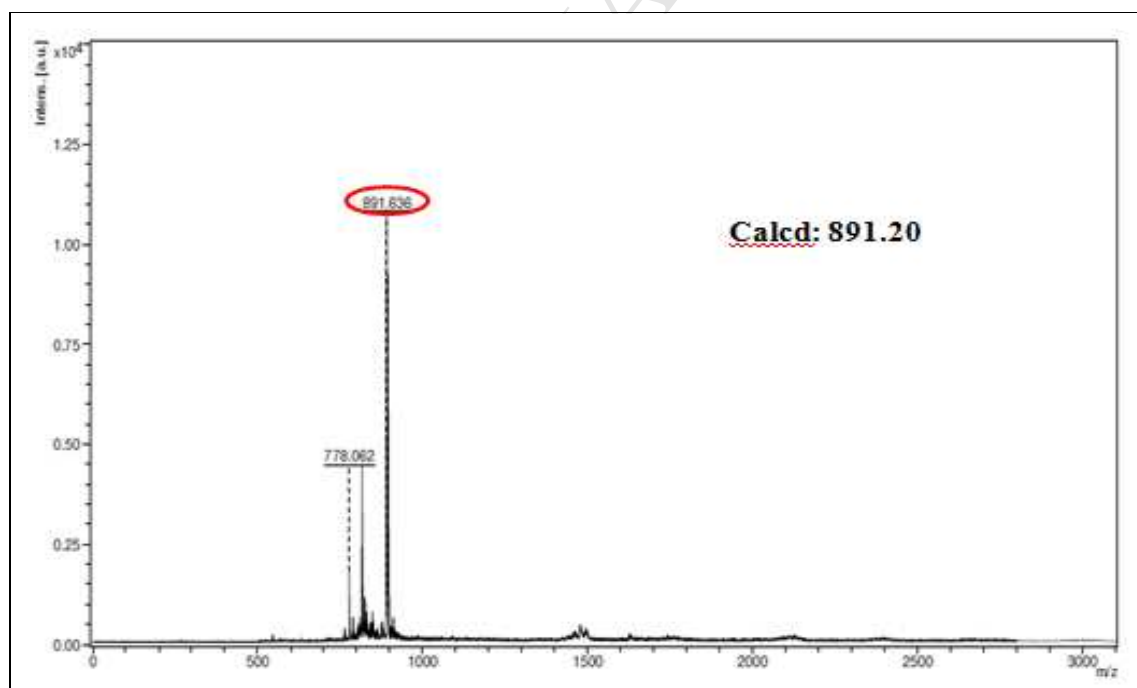


Fig. S30 MALDI-TOF-MS of ZnT(4-MeO)P(CN-COOH)

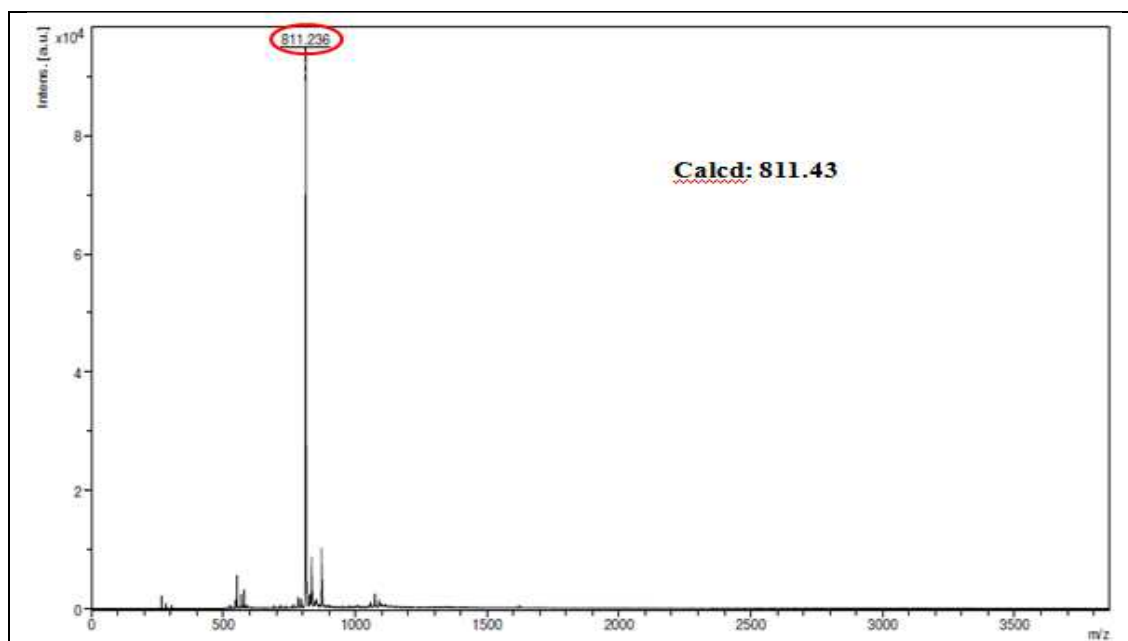


Fig. S31 MALDI-TOF-MS of H₂T(Mes)P(CHO)

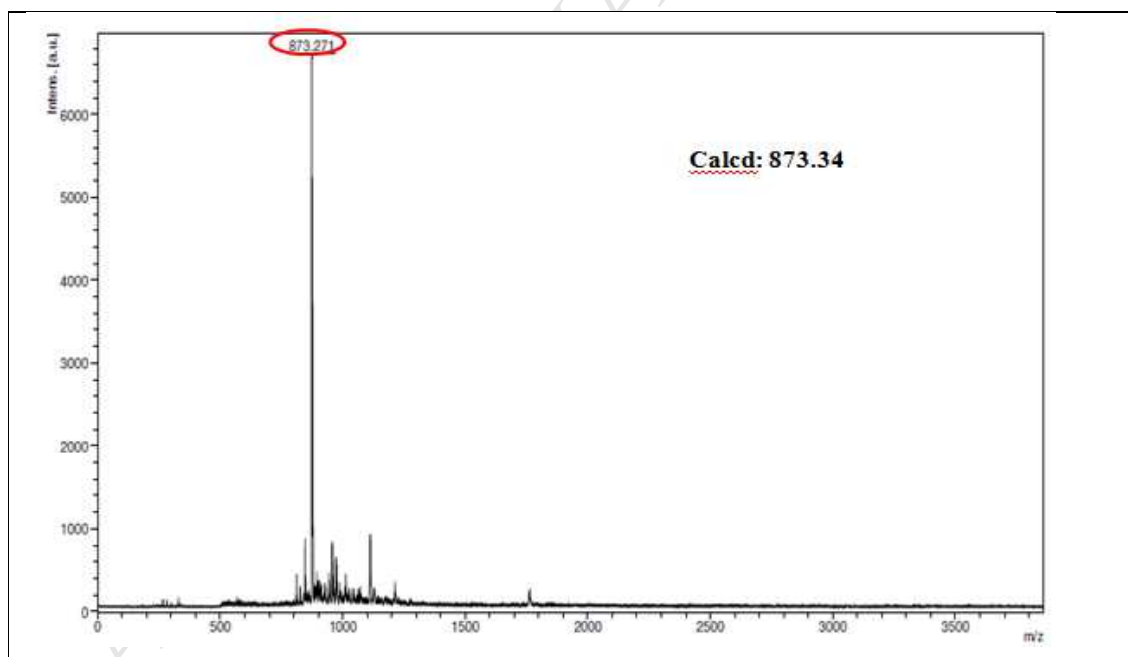


Fig. S32 MALDI-TOF-MS of ZnT(Mes)P(CHO)

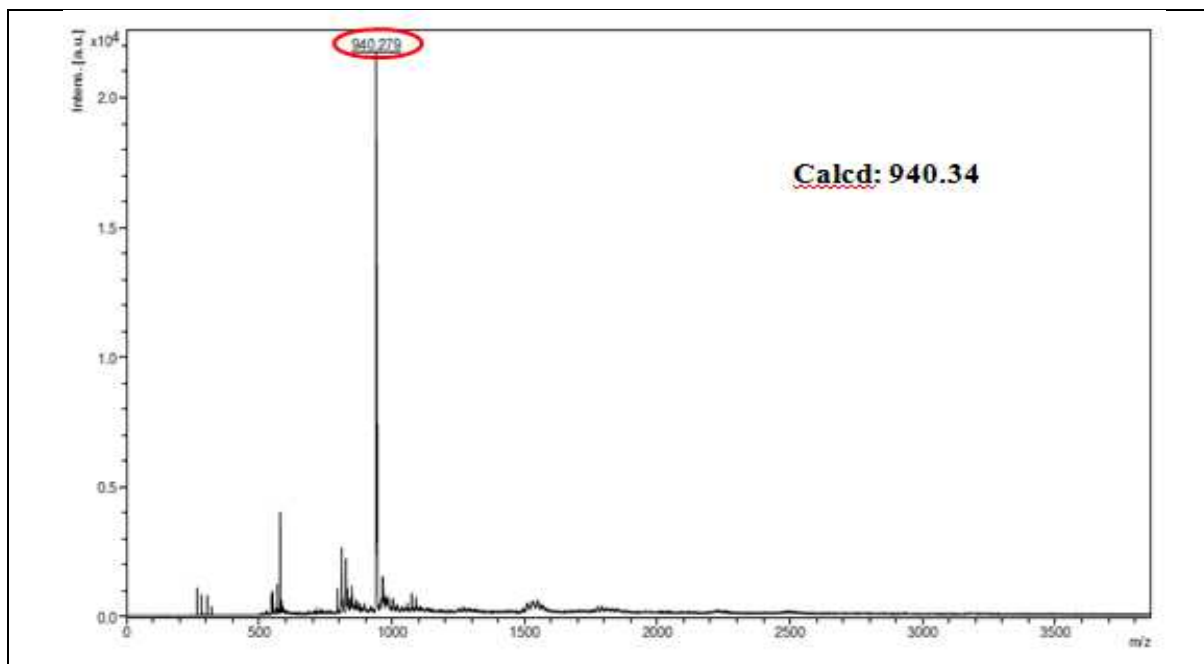


Fig. S33 MALDI-TOF-MS of ZnT(Mes)P(CN-COOH)

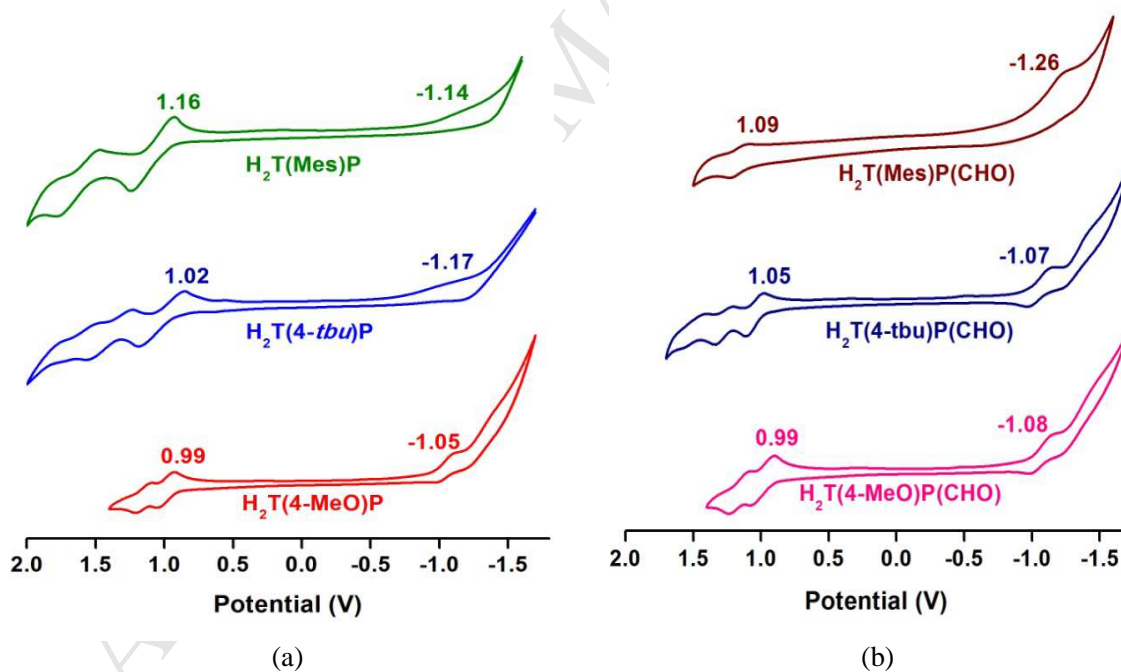


Fig. S34 Cyclic Voltammograms of (a) free base tetraarylporphyrins (b) free base mono-formylporphyrins, and (c) in CH_2Cl_2 at 298 K

Highlights for review:

- 1) Facile, easy synthesis of β -functionalized “push-pull” porphyrins and their characterization.
- 2) The Soret and Q band of Zn(II) porphyrin dyes were red-shifted (30-35 nm) and broadened as compared to ZnTPP.
- 3) The fluorescence quenching, decrement in quantum yield and lifetime reflected intramolecular charge transfer from donor to acceptor.
- 4) The HOMO-LUMO energy levels of Zn(II)porphyrin dyes suggest the feasibility of facile electron-transfer in DSSC.
- 5) ZnT(Mes)P(CN-COOH) displayed power conversion efficiency (PCE) of $\eta = 3.13\%$ whereas co-sensitization of this dye with N719 organic dye increased PCE efficiency up to 5.35%.